



**NLTERT – A Code for Computing the
Radiative Properties of Non-LTE Plasmas**

J.J. MacFarlane

December 1993

UWFDM-931

**FUSION TECHNOLOGY INSTITUTE
UNIVERSITY OF WISCONSIN
MADISON WISCONSIN**

**NLTERT – A Code for Computing the
Radiative Properties of Non-LTE Plasmas**

J. J. MacFarlane

Fusion Technology Institute
University of Wisconsin-Madison
1500 Johnson Drive
Madison, WI 53706

December 1993

UWFDM-931

Contents

1. Introduction	1.1
2. Statistical Equilibrium Model	2.1
3. Radiative Transfer Models	3.1
3.1. Escape Probability Model	3.1
3.2. Multifrequency, Multiangle Radiative Transfer Model	3.10
4. Atomic Physics Models	4.1
5. Input/Output File Descriptions	5.1
6. Namelist Input Variables	6.1
7. Subroutines	7.1
8. Common Blocks	8.1
9. Sample Calculations	9.1
9.1. Example 1: Thermal Spectrum for Aluminum	9.1
9.2. Example 2: 2-Level Atom	9.1
9.3. Example 3: K _α Absorption Spectrum for Aluminum	9.1

1. Introduction

Emission and absorption spectroscopy are often used to determine the physical conditions of laboratory and astrophysical plasmas. Absorption spectroscopy has been utilized in determining plasma temperatures and densities, as well as measure opacities, in laser-produced plasma experiments [1-7]. Emission spectroscopy is often used to deduce plasma conditions in Z-pinch plasmas and imploding inertial confinement fusion (ICF) targets [8]. In plasmas heated by intense light ion beams, x-ray emission lines arising from inner-shell transitions can be used to diagnose plasma conditions [9-12]. Proper interpretation of experimental spectra often requires detailed radiative and atomic physics models.

In this report, we describe the features of NLTERT — a code we have developed to investigate the radiative properties of high energy density plasmas. This is a non-LTE (LTE = local thermodynamic equilibrium) radiative transfer code, or collisional-radiative equilibrium (CRE) code, which can be used to calculate emission and absorption spectra, as well as radiative energy transport. The major features of the physics models have been described elsewhere [13-16], and only a brief overview of the models will be presented here. This report is intended to be a “users’ guide.” Thus, the focus here will be on the structure of the code and how to use it. A users’ guide for the atomic physics package which sets up atomic data files for the CRE code is presented elsewhere [17].

Given a temperature and density distribution for a plasma, NLTERT computes atomic level populations and resultant spectra for single- or multi-component plasmas. The models are 1-D, and work for planar, cylindrical, and spherical geometries. Opacity effects are considered in computing both the atomic level populations (via photoexcitation and photoionization) and the spectra. In addition, ion beam-induced ionization is considered in the statistical equilibrium equations to allow for the analysis of spectra obtained in intense light ion beam experiments.

Sections 2 through 4 of this report provide brief descriptions of the statistical equilibrium, radiative transfer, and atomic physics models. Input and output files are described in Section 5, while the namelist input used to set up a calculation is detailed in Section 6. The subroutines and common block descriptions are provided in Sections 7 and 8, respectively. Finally, a series of sample calculations is shown in Section 9.

2. Statistical Equilibrium Model

Atomic level populations are calculated by solving multilevel, steady-state atomic rate equations self-consistently with the radiation field and, if necessary, the ion beam properties. For multilevel systems, the rate equation for atomic level i can be written as:

$$\frac{dn_i}{dt} = -n_i \sum_{j \neq i}^{N_L} W_{ij} + \sum_{j \neq i}^{N_L} n_j W_{ji} = 0, \quad (2.1)$$

where W_{ij} and W_{ji} represent the depopulating and populating rates between levels i and j , n_i is the number density of level i , and N_L is the total number of levels in the system. For upward transitions ($i < j$),

$$W_{ij} = B_{ij} \bar{J}_{ij} + n_e C_{ij} + \beta_{ij} + n_e \gamma_{ij} + \mathcal{R}_{ij}, \quad (2.2)$$

while for downward transitions,

$$W_{ji} = A_{ji} + B_{ji} \bar{J}_{ji} + n_e D_{ji} + n_e (\alpha_{ji}^{RR} + \alpha_{ji}^{DR}) + n_e^2 \delta_{ji} + \Omega_{ji}, \quad (2.3)$$

where n_e is the electron density and \bar{J}_{ij} ($\equiv \int \phi_{ij}(\nu) J_\nu d\nu$) is the frequency-averaged mean intensity of the radiation field for a bound-bound transition. The rate coefficients in the above equations are:

A_{ij}	= spontaneous emission
B_{ij}	= stimulated absorption ($i < j$) or emission ($i > j$)
C_{ij}	= collisional excitation
D_{ij}	= collisional deexcitation
α_{ij}^{RR}	= radiative recombination
α_{ij}^{DR}	= dielectronic recombination
β_{ij}	= photoionization plus stimulated recombination (defined in Sec. 3)
γ_{ij}	= collisional ionization
δ_{ij}	= collisional recombination
\mathcal{R}_{ij}	= ion beam impact ionization
Ω_{ij}	= autoionization.

Atomic cross sections for the above terms are described briefly in Section 4. The last two terms, \mathcal{R}_{ij} and Ω_{ij} , are relevant for problems involving inner-shell ionization by intense ion beams. The ion beam-impact ionization rate coefficient can be written as:

$$\mathcal{R}_{ij} = J_B \sigma_{S,ij} (E_B),$$

where J_B is the ion beam current density, E_B is the beam energy (per particle), and $\sigma_S (E_B)$ is the ion-impact ionization cross section for ejecting an electron out of subshell S . The autoionization rate coefficient out of autoionizing level i is:

$$\Omega_{ij} = \left(\frac{1 - Y_i}{Y_i} \right) \sum_{j'} A_{ij'},$$

where A_{ij} is the spontaneous emission rate and Y_i is the fluorescence yield. NLTERT has recently been updated to use ion-impact ionization cross sections and autoionization rates (fluorescence yields) calculated by ATBASE [17] for individual transitions. Thus, it is not necessary to rely on configuration- or ion-averaged values as was done in previous studies.

In this detailed configuration accounting model each atomic level of a given gas species can in principal be coupled to any other level in that gas. This allows for modelling plasmas in which multiple ionization processes are important (such as non-protonic ion beams or Auger ionization due to x-rays). The degree of coupling between levels depends on how the atomic data files are generated by ATBASE.

The statistical equilibrium equations (Eq. (2.1)) depend on the atomic level populations in a nonlinear fashion (through the radiation intensity and electron density). Because of this, an iterative procedure is used to obtain atomic level populations which are self-consistent with the radiation field. At present, the coupled set of steady-state rate equations is solved using the LAPACK linear algebra package [18]. Besides inverting the statistical equilibrium equation matrix to obtain the level populations, LAPACK also contains algorithms for improving the condition of the matrix via scaling, as well as iterative refinement. The overall procedures for computing the level populations is as follows:

1. Make an initial guess for population distributions (e.g., LTE or optically thin plasma)
2. Compute radiative rate coefficients
3. Compute coefficients for statistical equilibrium matrix ($N_L \times N_L$)

4. Solve matrix for level populations
5. If new populations are consistent with previous iteration, calculation is complete; otherwise go back to step 2.

Steps 2 through 4 are performed one spatial zone at a time. This is possible because we employ an accelerated lambda iteration procedure (ALI) which utilizes the diagonal of the Λ -operator [19,20; see also Section 3].

To improve the rate of convergence for this iterative procedure we utilize an acceleration technique based on the work of Ng [21; see also 22, 20]. The Ng acceleration method is applied every several (typically 2 to 6) iterations to obtain updated solutions to the solution vector \mathbf{x} . In our case, the solution vector is the level population of a spatial zone. The “accelerated” solution is calculated from solutions obtained during the previous several iterations — that is, the evolution, or history, of the convergence becomes important. The accelerated solution vector after the n 'th iteration can be written as:

$$\mathbf{x}^n = \left(1 - \sum_{m=1}^M \alpha_m\right) \mathbf{x}^{n-1} + \sum_{m=1}^M \alpha_m \mathbf{x}^{n-m-1}, \quad (2.4)$$

where \mathbf{x}^{n-m} is the solution vector of the $(n-m)$ 'th iteration. The acceleration coefficients, α , are determined from the solution

$$\mathbf{A}\alpha = \mathbf{b}, \quad (2.5)$$

where the elements of \mathbf{A} and \mathbf{b} are given by:

$$\begin{aligned} A_{ij} &= \sum_{d=1}^D (\Delta x_d^n - \Delta x_d^{n-i})(\Delta x_d^n - \Delta x_d^{n-j}), \\ b_i &= \sum_{d=1}^D \Delta x_d^n (\Delta x_d^n - \Delta x_d^{n-i}), \end{aligned} \quad (2.6)$$

and

$$\Delta x_d^k \equiv x_d^k - x_d^{k-i}.$$

The quantity x_d^k refers to the d 'th element of \mathbf{x} on iteration cycle k . The order of the acceleration method, M , represents the number of previous cycles used to compute the accelerated solution for \mathbf{x} .

In our radiative transfer code M can be chosen to have a value from 2 to 4. It is found that using $M = 2$ provides very good acceleration to the converged solution. This method has proven to be particularly valuable in improving the computational efficiency of our radiative transfer simulations.

3. Radiative Transfer Models

NLTERT utilizes two radiative transfer models: (1) an angle- and frequency-averaged escape probability model, and (2) a multiangle, multifrequency model based on the second order form of the radiative transfer equation (Feautrier method) [23]. The advantage of the escape probability model is that it is faster. This is especially true in spherical geometry, where the Feautrier method solves the radiative transfer equation along a large number of impact parameters (approximately equal to the number of spatial zones). The advantage of the Feautrier method is accuracy. This method is second order accurate, while the escape probability model assumes the source function — and thereby the atomic level populations — are uniform throughout each spatial zone (this is sometimes referred to as the “flat flux approximation”). In addition, because it utilizes a multifrequency grid for each bound-bound transition, it can more accurately treat line transport in problems with a significant background continuum. For many practical applications the escape probability model works quite satisfactorily. The user can of course check this by comparing results of separate test calculations using the two models. Below we describe each model separately.

3.1. Escape Probability Model

In the escape probability model, the stimulated absorption and emission rates in Eqs. (2.2) and (2.3) can be written in terms of zone-to-zone coupling coefficients:

$$n_j^a B_{ji} \bar{J}_{ij} - n_i^a B_{ij} \bar{J}_{ij} = \begin{cases} -A_{ji} \sum_{e=1}^{N_D} n_j^e Q_{ji}^{ea} & (i < j) \\ A_{ij} \sum_{e=1}^{N_D} n_i^e Q_{ij}^{ea} & (i > j) \end{cases}$$

where Q^{ea} is defined as the probability a photon emitted in zone e is absorbed in zone a , n_i is the population density of level i , the superscripts e and a denote the emitting and absorbing zones, respectively, and N_D is the number of spatial zones. Our model utilizes a computationally efficient method for computing angle- and frequency-averaged escape probability coupling coefficients in planar, cylindrical, and spherical geometries for Doppler, Lorentz, and Voigt line profiles. (This method is based largely on the work of J. Apruzese et al. [24-26].)

Consider first the 1-D planar geometry shown in Fig. 3.1. The distance traversed as a photon travels from point 1 to point 2 is z_{12}/μ , where $\mu \equiv \cos \theta$ and θ is the angle between the direction of propagation and the normal to the slab surface. In this geometry,

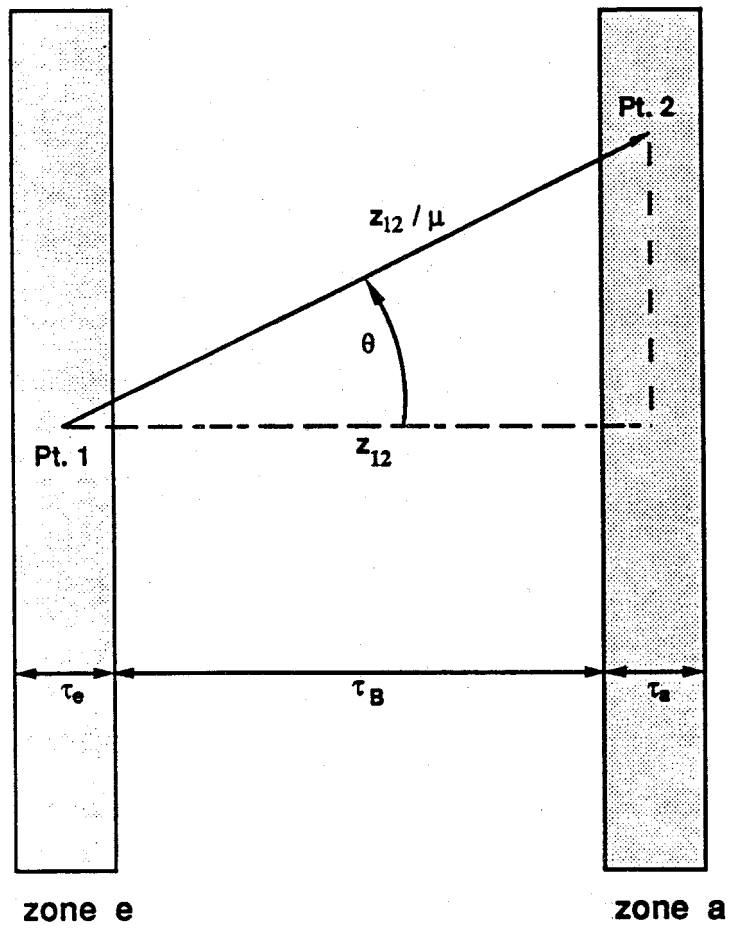


Figure 3.1. Schematic illustration of photon transport in planar geometry.

the angle- and frequency-averaged escape probability, \overline{P}_e , can be computed directly:

$$\overline{P}_e(\tau_c) = \int_0^1 P_e(\tau_c/\mu) d\mu, \quad (3.1)$$

where P_e is the frequency-averaged escape probability (described below). The probability a photon emitted in zone e traverses a depth τ_B between zones e and a , and is then absorbed in zone a is

$$Q^{ea} = \frac{1}{2\tau_e} \int_0^{\tau_e} [\bar{P}_e(\tau_B + \tau) - \bar{P}_e(\tau_B + \tau_a + \tau)] d\tau. \quad (3.2)$$

Note that τ_e , τ_B , and τ_a are the optical depths in the direction normal to the slab surface. The first term within the integral represents the probability a photon will get to the nearer surface of zone a without being absorbed, while the second term represents the probability the photon is absorbed before exiting the surface farther from zone e . The coupling coefficients are efficiently computed using analytic expressions.

Evaluation of the coupling coefficients in cylindrical and spherical geometries is more difficult because Eq. (3.1) is not valid and angle-averaged escape probabilities cannot be computed directly. For these geometries, it was found [25] that introducing a “mean diffusivity angle,” $\bar{\theta} \equiv \cos^{-1} \bar{\mu}$, for which

$$P_e\left(\frac{\tau}{\bar{\mu}}\right) \cong \int_0^1 P_e\left(\frac{\tau}{\mu}\right) d\mu, \quad (3.3)$$

leads to solutions that compare reasonably well with exact solutions. The meaning of the mean diffusivity angle is clarified in Fig. 3.2. The quantities τ_e , τ_a , and τ_B again represent the line center optical depths of the emitting and absorbing zones and the depth between them, respectively. In this case, however, the optical depths are computed along the ray defined by $\bar{\theta}$ and the midpoint of the emitting zone.

It can also be seen from Fig. 3.2 that additional geometrical complications arise when the absorbing zone is inside the emitting zone. To overcome this, while at the same time maintaining computational efficiency, we take advantage of the reciprocity relation:

$$N^i Q^{ij} = N^j Q^{ji}, \quad (3.4)$$

where N^i and N^j are the total number of absorbing atoms in zones i and j , respectively. (A proof of this relation is given in Ref. [25]). Thus, in cylindrical and spherical geometries the coupling coefficients are given by:

$$Q^{ea} = \frac{1}{\tau_e} \int_0^{\tau_e} [P_e(\tau_B + \tau) - P_e(\tau_B + \tau_a + \tau)] d\tau, \quad (3.5)$$

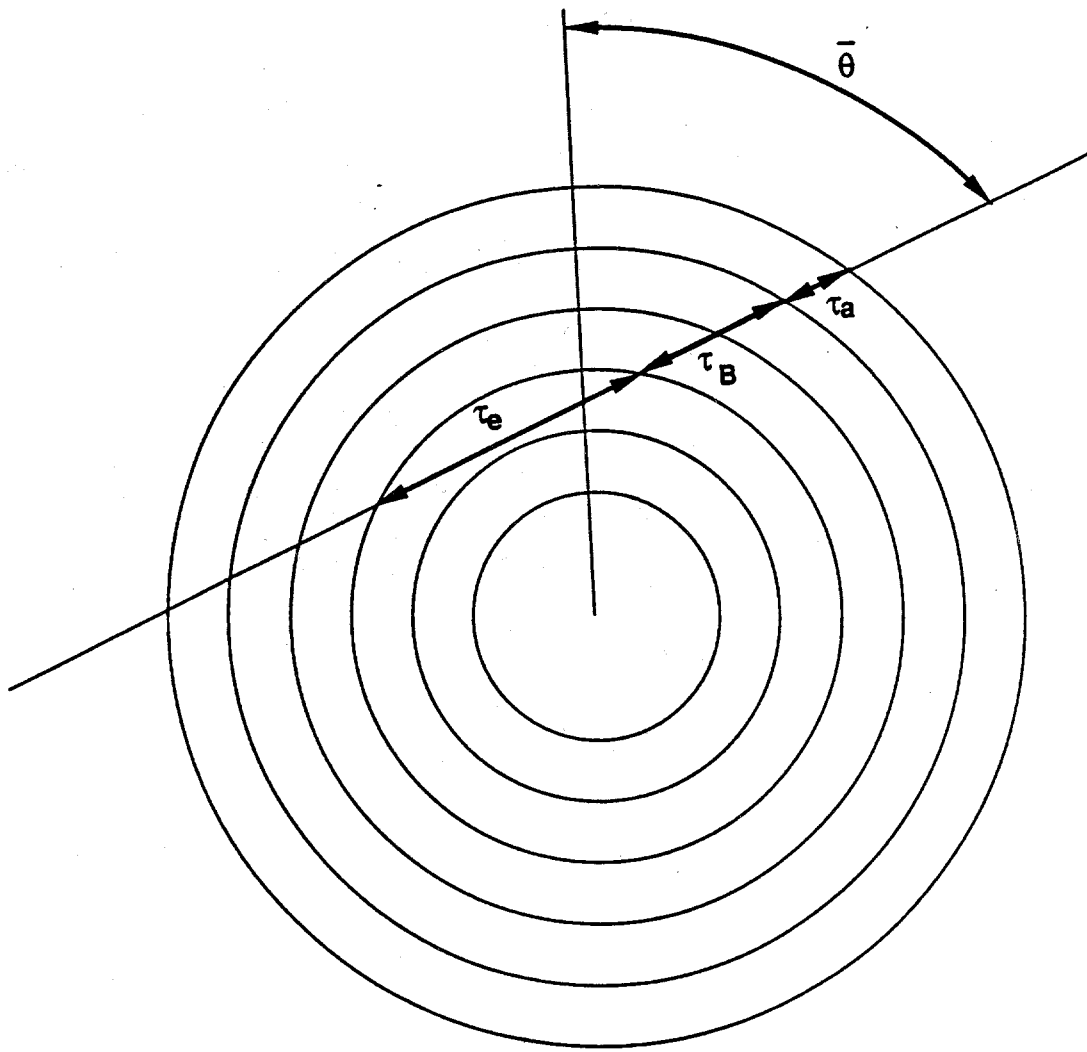


Figure 3.2. Schematic illustration of photon transport in cylindrical and spherical geometries.

where P_e is the non-angle-averaged escape probability. The Q^{ea} are calculated using Eq. (3.5) only for the cases when the absorbing zone is at a larger radius than the emitting zone. Otherwise, the reciprocity relation (Eq. (3.4)) is used. It has been shown [25] that using $\bar{\mu} = 0.51$ leads to solutions for 2-level atoms that are accurate to within 25% for a wide range of total optical depths.

The frequency-averaged probability a photon will traverse a distance equivalent to a line center optical depth τ_c is:

$$P_e(\tau_c) = \int_0^\infty \phi(\nu) e^{-\tau_\nu} d\nu, \quad (3.6)$$

where $\phi(\nu)$ is the normalized line profile ($\int \phi(\nu) d\nu = 1$), and

$$\tau_\nu = \tau_c \phi(\nu)/\phi(\nu_0).$$

The quantity ν_0 represents the frequency at line center.

The profiles considered for bound-bound transitions are:

$$\begin{aligned} \text{Doppler : } \phi(\nu) &= (\pi^{1/2} \Delta\nu_D)^{-1} e^{-x_D^2}, & x_D &= \frac{\nu - \nu_0}{\Delta\nu_D} \\ \text{Lorentz : } \phi(\nu) &= \frac{4}{\Gamma} \frac{1}{1+x_L^2}, & x_L &= \frac{4\pi}{\Gamma} (\nu - \nu_0) \\ \text{Voigt : } \phi(\nu) &= (\pi^{1/2} \Delta\nu_D)^{-1} H(a, x_D), & a &= \frac{\Gamma}{4\pi \Delta\nu_D}. \end{aligned} \quad (3.7)$$

The parameter Γ can be interpreted as the reciprocal of the mean lifetimes of the upper and lower states, $\Delta\nu_D$ is the Doppler width of the line, and

$$H(a, x_D) = \frac{a}{\pi} \int_{-\infty}^\infty \frac{e^{-y^2}}{(x_D - y)^2 + a^2} \quad (3.8)$$

is the Voigt function[23].

In evaluating the escape probability integrals we use an approach similar to that of Apruzese et al. [24-26]. Simple analytic fits to accurate numerical solutions to the frequency-averaged escape probabilities were obtained for each profile. For bound-bound transitions, complete frequency redistribution is assumed; i.e., the emission and absorption profiles are identical.

For Doppler profiles we use:

$$P_e(\tau_c) = \begin{cases} 2.329 [\tan^{-1}(0.675\tau_c + 0.757) - \tan^{-1}(0.757)], & \tau_c \leq 5.18 \\ 0.209 + 1.094 [\ln \tau_c]^{1/2}, & \tau_c > 5.18, \end{cases} \quad (3.9)$$

while for Lorentz profiles we use:

$$P_e(\tau_c) = \begin{cases} 1.707 \ln(1 + 0.586 \tau_c), & \tau_c \leq 5.18 \\ -0.187 + 1.128 \tau_c^{1/2}, & \tau_c > 5.18. \end{cases} \quad (3.10)$$

For Voigt profiles, the escape probability integrals were fitted to two different regimes of the Voigt broadening parameter a . For $a < 0.49$,

$$P_e(\tau) = \begin{cases} (1 + 1.5\tau)^{-1} & (\tau \leq 1), \\ 0.4\tau^{-1} & (1 < \tau \leq \tau_c), \\ 0.4(\tau_c\tau)^{-1/2} & (\tau > \tau_c), \end{cases} \quad (3.11)$$

where

$$\tau_c \equiv \frac{0.83}{a(1 + a^{1/2})}.$$

For $a \geq 0.49$,

$$P_e(\tau) = \begin{cases} (1 + \tau)^{-1} & (\tau \leq 1), \\ 0.5 \tau^{-1/2} & (\tau > 1). \end{cases} \quad (3.12)$$

The fits for Voigt profiles are typically accurate to about 20%, although errors of up to 40% can occur. Note, however, that in our model the frequency-averaged escape probability integrals are used only to compute the level populations self-consistently with the radiation field. The frequency-dependent spectral calculations do not directly use frequency-averaged escape probabilities.

We now discuss the transport of bound-free radiation in the context of the escape probability model. The frequency-averaged escape probability is obtained by averaging the attenuation factor, $e^{-\tau_\nu}$, over the emission profile ϕ_E :

$$P_e(\tau_0, \alpha_0) = \int_{\nu_1}^{\infty} \phi_E(\nu, \alpha_0) \exp(-\tau_\nu) d\nu, \quad (3.13)$$

where

$$\phi_E(\nu, \alpha_0) = \frac{\exp(-h\nu/kT_e)}{\nu E_1(\alpha_0)}$$

and

$$\alpha_0 \equiv h\nu_1/kT_e.$$

The optical depth and frequency at the photoionization edge are τ_0 and ν_1 , respectively, τ_ν is the optical depth at frequency ν , T_e is the electron temperature, and $E_1(x)$ represents the exponential integral of order 1. The quantities h and k as usual refer to the Planck constant and Boltzmann constant, respectively.

As in the case of line transport, frequency-averaged escape probabilities have been fitted to simple analytic functions to allow for computationally efficient solutions. The curve fits are given by:

$$P_e(\tau_0, \alpha_0) = \begin{cases} e^{-\gamma_1 t} & , \quad t \leq 1.0 \\ t^{-1/3} \exp[-\gamma_1 - \gamma_2(t^{1/3} - 1)] & , \quad t > 1.0 \end{cases} \quad (3.14)$$

where

$$\begin{aligned} \gamma_1(\alpha_0) &= 2.01\alpha_0 - 1.23\alpha_0^{3/2} + 0.210\alpha_0^2, \\ \gamma_2(\alpha_0) &= 1.01\alpha_0 + 0.0691\alpha_0^{3/2} - 0.0462\alpha_0^2, \end{aligned}$$

and $t \equiv \tau_0/3$. The fits are accurate to about 15% over a wide range of parameter space: $0.3 < \alpha_0 < 10$ and values of τ_0 such that $P_e(\tau_0, \alpha_0) \geq 10^{-5}$.

The photoionization rate in zone a is obtained by summing the recombinations over all emitting zones e . Thus, the photoionization rate (corrected for stimulated recombinations) from lower level ℓ to upper level u can be written as:

$$\begin{aligned} \beta_{\ell u} &= 4\pi \int_{\nu_o}^{\infty} \frac{\alpha_\nu^{bf}}{h\nu} J_\nu^a \left(1 - \left(\frac{n_u^a}{n_\ell^a} \right) \left(\frac{n_\ell^a}{n_u^a} \right)^* e^{-h\nu/kT_e} \right) d\nu \\ &= \sum_{e=1}^{N_D} N_u^e n_e^e \alpha_{rr}^e Q^{ea}, \end{aligned} \quad (3.15)$$

where α_ν^{bf} is the photoionization cross section, J_ν is the radiation mean intensity, $(n_\ell/n_u)^*$ refers to the LTE population ratio [23], α_{rr}^e is the radiative recombination rate coefficient for zone e , n_e^e is the electron density in zone e , and N_D is the total number of spatial zones in the plasma.

Frequency-dependent spectra are computed in the escape probability model as follows. We first compute the opacities and optical depths in each spatial zone from all possible sources and consider the contributions from free-free (Bremsstrahlung), bound-free (photoabsorption), and bound-bound (line) transitions. The optical depth at frequency ν in zone d , is related to the opacity by:

$$\begin{aligned}\tau_{\nu,d} &= \int_{z_{min}}^{z_{max}} \chi_{\nu}(z) dz \\ &= \chi_{\nu,d} \Delta z_d,\end{aligned}\quad (3.16)$$

where the opacity in zone d , $\chi_{\nu,d}$, is assumed to be constant throughout the zone, and Δz_d is the zone thickness. The opacity can be written as [23]:

$$\begin{aligned}\chi_{\nu} &= \sum_j n_e n_{j+1} (1 - e^{h\nu/kT}) \alpha^{ff}(\nu) \\ &+ \sum_j \sum_n [n_{nj} - n_{nj}^* e^{-h\nu/kT}] \alpha_n^{bf}(\nu) \\ &+ \sum_j \sum_n \sum_{m>n} \left[n_{nj} - \left(\frac{g_{nj}}{g_{mj}} \right) n_{mj} \right] \alpha_{mn}^{bb}(\nu),\end{aligned}\quad (3.17)$$

where the index j refers to the ionization stage, n and m refer to the excitation levels, g_{nj} and g_{mj} are the statistical weights, n_{nj} is the number density of atoms in level n of ionization stage j , and n_{j+1} is the number density of atoms in ionization stage $j + 1$ summed over all excitation levels. The quantity n_{nj}^* is the LTE population of state n_{nj} computed using the actual ion density of the upper ionization stage. The first term in Eq. (3.17) is the contribution from free-free absorption, the second is from bound-free absorption, and the third is due to bound-bound absorption. The free-free cross section is given by

$$\alpha^{ff}(\nu) = \left(\frac{4e^6}{3ch} \right) \left(\frac{3\pi}{3km_e} \right)^{1/2} \overline{g_{ff}} Z_{eff}^2 T^{-1/2} \nu^{-3}, \quad (3.18)$$

where e and m_e are the electron charge and mass, respectively, c is the speed of light, $\overline{g_{ff}}$ is the free-free Gaunt factor [27], and Z_{eff} is the effective charge.

The bound-free cross section has the form:

$$\alpha^{bf}(\nu) = \alpha^{bf}(\nu_1) \left\{ \beta \left(\frac{\nu_1}{\nu} \right)^s + (1 - \beta) \left(\frac{\nu_1}{\nu} \right)^{s+1} \right\}, \quad \nu \geq \nu_1, \quad (3.19)$$

where ν_1 is the cutoff frequency, and β , s , and $\alpha^{bf}(\nu_1)$ are obtained by fitting to Hartree-Fock cross section for electrons in each subshell of each atomic level. The bound-bound cross section is given by

$$\alpha^{bb}(\nu) = \left(\frac{\pi e^2}{m_e c} \right) f_{nm} \phi_\nu, \quad (3.20)$$

where f_{nm} is the oscillator strength and ϕ_ν is the normalized line profile ($\int \phi_\nu d\nu = 1$).

After the total optical depth for each spatial zone is calculated, the frequency-dependent flux at the plasma boundary is computed as follows. The flux at the surface due to photons emitted in zone d , $F_{\nu,d}$, can be written in terms of the plasma emissivity of the zone, $\eta_{\nu,d}$:

$$F_{\nu,d} = \frac{4\pi \eta_{\nu,d} \Delta V_d}{A} \mathcal{A}_{\nu,d}, \quad (3.21)$$

where ΔV_d is the volume of zone d , and A is the area of the plasma boundary. The attenuation factor, $\mathcal{A}_{\nu,d}$, represents the attenuation due to all other zones along the path to the boundary. The path from the emitting zone to the boundary is defined by the mean diffusivity angle. The optical depths for each zone are computed along this path. The attenuation factor is then obtained by averaging over the emitting zone:

$$\mathcal{A}_{\nu,d} = \frac{1}{\Delta \tau_{\nu,d}} \int_{\tau_{\nu,d}}^{\tau_{\nu,d} + \Delta \tau_{\nu,d}} e^{-\tau_\nu} d\tau_\nu. \quad (3.22)$$

where τ_d is the optical depth from the plasma boundary to the closer boundary of zone d . The emissivity can be written as [23]:

$$\begin{aligned} \eta_\nu &= \left(\frac{2h\nu^3}{c^2} \right) \sum_j \left\{ n_e n_{j+1} e^{-h\nu/kT} \alpha^{ff}(\nu) \right. \\ &\quad + \sum_n n_{nj}^* e^{-h\nu/kT} \alpha_n^{bf}(\nu) \\ &\quad \left. + \sum_n \sum_{m>n} \left(\frac{g_{nj}}{g_{mj}} \right) n_{mj} \alpha_{mn}^{bb}(\nu) \right\}. \end{aligned} \quad (3.23)$$

Note that the radiation produced by one type of transition can be significantly attenuated by other types of transitions. For instance, continuum emission can decrease abruptly near the cores of optically thick lines and photoabsorption edges. We note,

however, that this interaction of the radiation field for different transitions is not fully accounted for when calculating the level populations. We do not expect this to be a serious deficiency in the model for most types of plasma diagnostics.

3.2. Multifrequency, Multiangle Radiative Transfer Model

An alternative approach for computing radiative transfer in NLTERT is a multifrequency, multiangle model based on the second order form of the transfer equation. The model, which has been developed for planar and spherical geometries, is more accurate and can better model a wider class of problems (e.g., line transport in the presence of a significant continuum background, or large density and/or temperature gradients). The trade-off is of course that the required computational time is greater. This is particularly true in the case of spherical geometry, where the tangent ray method employed requires that the number of angles for which the radiative transfer equation is solved is comparable to the number of spatial grid points.

The second order form of the radiative transfer equation in planar geometry can be written as [23]:

$$\mu^2 \frac{\partial^2 u_{\mu\nu}}{\partial \tau_\nu^2} = u_{\mu\nu} - S_\nu, \quad (3.24)$$

where

$$u(z, \mu, \nu) = \frac{1}{2} [I(z, \mu, \nu) + I(z, -\mu, \nu)]$$

is the average of the specific intensity in the positive and negative μ directions, μ is the cosine of the angle between the direction the photon propagates and the normal to the slab, τ_ν is the optical depth at frequency ν , and S_ν is the source function ($= \eta_\nu / \kappa_\nu$).

Discretizing Eq. (3.24) onto the optical depth grid τ_d ($d = 1, \dots, N_D$) leads to the tridiagonal system of equations [28]:

$$-A_d u_{d-1} + B_d u_d - C_d u_{d+1} = S_d, \quad (3.25)$$

where second-order differencing provides for $2 \leq d \leq N_D$:

$$\begin{aligned} A_d &= \frac{2}{\Delta \tau_{d-1} (\Delta \tau_{d-1} + \Delta \tau_d)}, \\ B_d &= 1 + \frac{2}{\Delta \tau_d \Delta \tau_{d-1}}, \\ C_d &= \frac{2}{\Delta \tau_d (\Delta \tau_{d-1} + \Delta \tau_d)}, \end{aligned}$$

where $\Delta\tau_d = \tau_{d+1} - \tau_d$. The values of A_d , B_d , and C_d for $d = 1$ and N_D depend on boundary conditions.

A key point to note is that this approach is second-order accurate. The solution of u_d depends on the value of the source function at d and $d \pm 1$. By comparison, the escape probability model is numerically less accurate because the source function is assumed to be uniform within each zone.

The photoexcitation and photoionization rates used in the statistical equilibrium equations are obtained by integrating over angle and frequency. Expressions for these rates are given in Ref. [20]. In planar geometry the angle grid is defined by Gaussian integration abscissas and weights (see, e.g., [29]). In spherical geometry the transfer equation is solved along rays which are tangent to the radius of each zone of the spatial grid (see Fig. 3.3). This approach is commonly used to solve spherical radiative transfer problems [23,30].

The frequency grid for lines is set up so that there are equally-spaced points in each line core and logarithmically-spaced points in the line wings. Typically the core region has a frequency interval of several Doppler widths. About 5 frequency points are used for the core and 10-15 are used for the wings. These parameters can be adjusted by the user. For bound-free transitions we choose frequencies such that y -values ($y \equiv \nu_1/\nu$; $\nu_1 \equiv$ frequency of absorption edge) are evenly spaced.

To accelerate the convergence to a solution in which the statistical equilibrium and radiative transfer equations are simultaneously satisfied, we employ an accelerated lambda iteration procedure in which the diagonal of the “ Λ -operator” is included in an implicit fashion in the statistical equilibrium equations. The mean intensity \bar{J} can be expressed in terms of the Λ -operator in planar geometry as [23,28]:

$$\begin{aligned}\bar{J}(\vec{r}) &= \bar{\Lambda}[S(\vec{r})] = \frac{1}{2} \int_0^\infty d\nu \phi_\nu \left[\int_0^1 d\mu \int_{\tau_\nu}^{T_\nu} S_\nu(t) e^{-(t-\tau_\nu)/\mu} \frac{dt}{\mu} \right. \\ &\quad \left. + \int_{-1}^0 d\mu \int_0^{\tau_\nu} S_\nu(t) e^{-(\tau_\nu-t)/\mu} \frac{dt}{\mu} \right].\end{aligned}$$

In the context of the escape probability model, the diagonal of the Λ -operator corresponds to the probability a photon emitted in a spatial zone is reabsorbed in the same zone before it escapes.

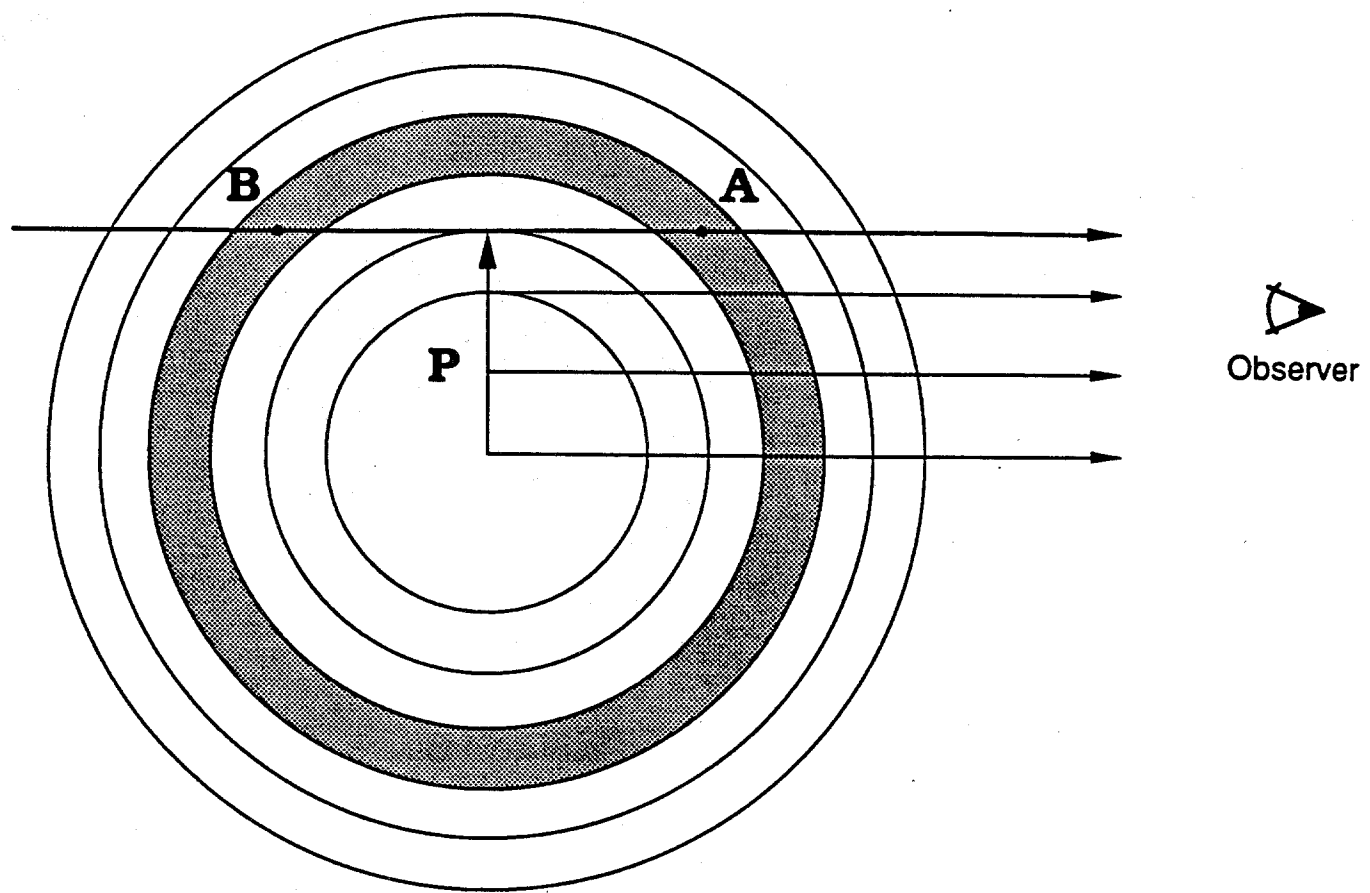


Figure 3.3. Illustration of spatial grid used to solve radiative transfer equation in spherical geometry. The impact parameters are tangent to the spherical shells. The radiation field is determined at points defined by the intersection of the rays and the spherical shells.

In the multifrequency radiation transport model of NLTERT, the matrix elements of the Λ -operator are calculated using the method recently proposed by Rybicki and Hummer [28], who showed that the diagonal elements of the Λ -operator can be calculated very efficiently using the matrix coefficients used to calculate the radiation intensity. A more detailed description of this technique is presented elsewhere [20].

4. Atomic Physics Models

Atomic structure calculations for energy levels are performed using a configuration interaction (CI) model using Hartree-Fock wavefunctions [17,31]. An L-S coupling scheme is used to define the angular momentum coupling of electrons. Rate coefficients for collisional and radiative transitions are calculated as follows. Collisional excitation and ionization rates are computed using a combination of semiclassical impact parameter, Born-Oppenheimer, and distorted wave models [32-34]. The corresponding inverse processes were specified from detailed balance arguments. Rate coefficients for dielectronic recombination are computed using a Burgess-Mertz model [35] in conjunction with Hartree-Fock energies and oscillator strengths. Photoionization cross sections and radiative recombination rates are obtained from Hartree-Fock calculations. Ion beam impact ionization of target *K*-shell and *L*-shell electrons are calculated for each ionization stage using a plane wave Born approximation model with corrections for Coulomb deflection, perturbations to the binding energy due to the incident projectile, and relativistic effects for target wavefunctions [36,37]. Details of the atomic physics calculations are given elsewhere [17,31].

5. Input/Output File Descriptions

The NLTERT code uses up to 6 types of input files, 7 output files, and 2 scratch files. The files are listed in Table 5.1, along with their default logical unit numbers (LUN), names (for UNIX systems), types, and a brief description of their contents. (Note that the LUNs and file names can be easily modified in the block data routine BDATA.) For each plasma species, up to four input files are required containing atomic data computed by the ATBASE suite of atomic physics codes [17]. Two of these files (LUNs 4 and 8) are required for all calculations. LUN 4 contains data for atomic level energies, oscillator strengths, collisional (electron impact) rate coefficients, and dielectronic recombination rate coefficients. LUN 8 contains photoionization cross section data. For calculations with ion beam-induced inner-shell ionization, two additional atomic data files are required for each target material (LUNs 9 and 10). LUN 9 contains ion impact ionization cross sections, while LUN 10 contains Auger rates and fluorescence yields.

Most parameters defining a problem are specified in the namelist input file (LUN 2). Details concerning variable names and definitions are given in Section 6.

To set up the target plasma temperature and density distributions, the user has the option of: (1) using namelist input, or (2) using results from hydrodynamics output. The latter option is chosen by setting ISW(44) > 0, in which case the hydrodynamics output is read in from LUN 45 by subroutine DHYDRO. The file name and current format options for reading the hydrodynamics data can be seen by examining DHYDRO. This subroutine can be easily modified to read in other formatted data.

Most of the useful output is written to 3 files: LUNS 6, 18, and 19. LUN 6 contains the descriptive output, including results for atomic level populations, ionization distributions, and line radiation power densities. LUN 18 contains plottable data for the flux vs. photon energy, while LUN 19 contains plot data for the optical depth vs. photon energy. The spectral properties are computed and written to LUNs 18 and 19 in subroutines SPECT1, SPECT2, and SPECT3.

Several other output files provide results that can be used to analyze a problem. LUNs 41 and 42 contain transition rate information, which can be used to determine the most important transitions which populate and depopulate the various atomic levels. LUN 3 is used to write warning messages, the purpose of which is used to warn the user of potential problems that may have occurred during the calculation without stopping the calculation. LUN 11 provides results for 2-level atom benchmark calculations. (A sample calculation involving a 2-level atom calculation is given in Sec. 9.)

Table 5.1. Input/Output Files

Default Unit Number	Default Name (UNIX)	Type	Description
2	rt.imp	Input	Namelist input
3	rt.warnings	Output	Warning messages which occur during run time
4	rt.atom.dat.NN	Input	Atomic structure data (energy levels, oscillator strengths, collisional rate coefficients)
6	rt.out	Output	Standard output (level populations, ionization distributions, line radiation power densities)
8	pixsec.dat.NN	Input	Photoionization cross sections
9	beam.AABB.xsec.NN	Input	Beam impact ionization cross sections
10	auger.atom.dat.NN	Input	Auger rate and fluorescence yields
11	2level.dat	Output	Results from 2-level atom benchmark calculations
18	rt.plot.08	Output	Plot file for frequency-dependent fluxes
19	rt.plot.09	Output	Plot file for frequency-dependent optical depths
41	rate1	Output	Transition rate tables
42	rate2	Output	Rate coefficient tables
45	—	Input	Plasma conditions from hydrodynamic simulations
54	aul.scratch	Scratch	Scratch file
55	rt.scratch	Scratch	Scratch file

NN = atomic number of target plasma

AA = atomic element symbol of beam projectile

BB = ionization stage of beam projectile

(e.g., LUN 9 would be ‘beam.Hy02.xsec.13’ for Al irradiated by a proton beam)

6. Namelist Input Variables

The user defines the parameters of a problem with the namelist input file. Through it, the user specifies the plasma properties, atomic model, spectral grid, radiative transfer model, and ion beam parameters (if necessary). In addition, the user can specify the types of plot output desired, and request the printing of various debugging output. Table 6.1 lists each of the namelist variable names, along with their type, dimensions, units, default values, and a brief description of their use. Comments can be inserted in the namelist input file to aid the user. Lines starting with ‘c’ in the namelist input file are considered comments. Note that the ‘c’ must be in the first column, and must be followed by a space.

The spatial grid is most easily set up using the automatic zoning algorithm, in which case IGEOM, NZONES, RADMIN, RADMAX, and DRADMN define the grid (DRAD is not used in this case). For isothermal, isochoric plasmas, the user simply specifies the ion density and electron temperature for each zone. Note that the electron and ion temperatures are assumed to be equal. To use temperature and density distributions from hydrodynamics simulations, the user should set ISW(44) or ISW(45) > 0, and set up input files in the proper format. (See subroutine DHYDRO for details of formatting and file specification; the user may wish to modify this routine to read other formatted temperature and density data.) The temperatures and densities for the radiative transfer grid are then determined by interpolation from the hydrodynamics grid. The parameter TDENDL is used to specify the total “column density” ($n \cdot \Delta L$); this ensures, for example, that the total mass per unit area be conserved in an expanding foil calculation.

The atomic model parameters specify the distribution of atomic species in the plasma. Homogeneous mixtures as well as multilayered target plasmas can be modelled. Examples of this are shown in Table 6.1. Input files for each atomic species are automatically read in based on the atomic numbers specified (ATOMNM). MXIZCH can be used to limit the maximum change for transitions; e.g., multiple ionization effects from intense ion beams can be ignored by setting MXIZCH=1.

The selection of atomic levels included in the NLTERT calculation is done through the variable ISELCT. This is a two-dimensional array arranged as [atomic level index, gas species]. By default, no levels are selected (all elements are zero). The user selects levels from the atomic data file (LUN 4) for each plasma species by setting the corresponding ISELCT array element to 1. For example, if one wishes to include level 85 from gas

species 1, one simply sets ISELCT(85,1)=1. It is often useful to set up the selection process ion by ion. Thus, if level 85 were the ground state of some ion, the lowest 20 energy levels of that ion could be selected by setting ISELCT(85,1)=20*1. Examples of this are provided in Section 9.

The variable ILINEP (listed under Radiative Transfer Parameters) is used to set the line profile type. For laboratory plasmas, a Voigt profile should generally be used. Natural, Doppler, and Stark broadening effects are automatically included in the calculation. ISW(7) and ISW(8) are used to specify whether photoexcitation and photoionization be considered in the statistical equilibrium equations. ISW(4) and ISW(5) indicate the choice of radiative transfer model: angle- and frequency-averaged escape probability model or multiangle, multifrequency model. The last 7 variables listed under the Radiative Transfer Parameters heading are used in the multifrequency radiative transfer model. The default values should be sufficient for laboratory plasma calculations.

The effects of an intense light ion beam can be modelled in NLTERT calculations. At present, it is best to set ISW(37)=3. This model utilizes ATBASE [17] atomic physics tables of ion beam impact ionization cross sections, as well as Auger rates and fluorescence yields. In this case, the proton impact ionization rate coefficient (PIMPIN) need not be specified by the user as the rate is automatically calculated for each atomic level based on the ion beam energy (EBEAM) and current density (CURDEN).

By default, the calculation of atomic level populations is performed by solving multilevel statistical equilibrium equations which include both collisional and radiative terms. However, the user can specify that LTE populations be computed by setting ISW(6)=3. ISW(6) is also used to specify the initial guess at the populations (see Section 2 for description of iterative procedure). In addition, transition rates for each type of process can be adjusted (or set to zero) by redefining CON(42) through CON(49).

Table 6.1. Namelist Input Variables

Variable Name	Type	Dimensions	Units	Default Value	Description
PLASMA, GRID PARAMETERS					
IGEOM	I*4	—	—	1	Coordinate index (1 – planar, 2 – cylindrical, 3 – spherical)
NZONES	I*4	—	—	0	Number of spatial zones (Maximum number = MXZONS)
RADMIN	R*8	—	cm	0.	Minimum radius or position
RADMAX	R*8	—	cm	0.	Maximum radius or position
DRADMN	R*8	—	cm	0.	Width of zone nearest the outer plasma boundary
DRAD	R*8	NZONES	cm	0.	Zone widths (not needed when using automatic zoning)
DENSNN	R*8	NZONES	cm ³	0.	Total ion density
TEMPEL	R*8	NZONES	eV	0.	Electron temperature
TDENDL	R*8	—	—	0.	Total column density ($\equiv \int_o^L n_{\text{ion}}(r) dr$) (Used to scale hydrodynamic density distributions to maintain correct target mass)

Variable Name	Type	Dimensions	Units	Default Value	Description
ATOMIC MODEL PARAMETERS					
NGASES	I*4	—	—	1	Number of gas species (maximum number = MXGASS)
ATOMNM	R*8	NGASES	—	0.	Atomic number
ATOMWT	R*8	NGASES	amu	0.	Atomic weight
MXIZCH	I*4	—	—	999	Maximum ionization change considered for transitions
FRACSP	R*8	NZONES, NGASES	—	1 for igas=1 0 for igas>1	Fractional concentration of gases in each zone
Example for homogeneous binary plasma with 20 zones:					
FRACSP(1,1) = 20*0.5					
FRACSP(1,2) = 20*0.5					
Example for layered plasma:					
FRACSP(1,1) = 10*1., 10*0.					
FRACSP(1,2) = 10*0., 10*1.					
Array to select atomic levels from atomic data files					
ISELCT	I*4	MXLVLI, MXGASS	—	0	1 ⇒ on (or select); 0 ⇒ off (default)

SPECTRAL CALCULATION PARAMETERS

Variable Name	Type	Dimensions	Units	Default Value	Description
IPLOT	I*4	—	—	0	Select as follows IPLOT (1) = 1: compute spectral flux using escape probability radiative transfer model IPLOT (1) = 2: compute spectral flux using multiangle, multifrequency radiative transfer model IPLOT (1) = 3: compute spectral intensity along a specified line of sight defined by XMULOS using multiangle, multifrequency radiative transfer model IPLOT (2) ≠ 0: print out source function distributions for 2-level atom calculations IPLOT (8) = 1: print out photon energies and fluxes IPLOT (8) = 2: print out log ₁₀ values of photon energies and fluxes IPLOT (9) = 1: print out photon energies and optical depths IPLOT (9) = 2: print out log ₁₀ values of photon energies and optical depths
NFRQFF	I*4	—	—	100	Number of frequency points for continuum
NFRQBB	I*4	—	—	5	Number of frequency points for each line
HVMIN	R*8	—	eV	1.0	Minimum frequency for spectral grid
HVMIN	R*8	—	eV	5000.	Maximum frequency for spectral grid
XMULOS	R*8	—	—	1.0	Cosine of angle used for line of sight if IPLOT (1) = 3

Variable Name	Type	Dimensions	Units	Default Value	Description
ILINEP	I*4	—	—	1	Line profile type (1 \Rightarrow Doppler; 2 \Rightarrow Lorentz; 3 \Rightarrow Voigt)
XMUBAR	R*8	—	—	0.51	Cosine of angle used for angle-averaged escape probability model
ISW (7)	I*4	100	—	0	Compute photoexcitation if equal to 1
ISW (8)	I*4	100	—	0	Compute photoionization if equal to 1
ISW (5)	I*4	100	—	0	If 0, use escape probability model for photoexcitation calculation; if 1, use multifrequency model for photoexcitation calculation
ISW (4)	I*4	100	—	0	If 0, use escape probability model for photoionization calculation; if 1, use multifrequency model for photoionization calculation
NFLINE	I*4	—	—	5	Number of frequency points for each line (sum for core and wings; used to compute photoexcitation rate)
NFPIZ0	I*4	—	—	5	Number of frequency points for each bound-free transition (used to compute photoionization rates)
NFCORE	I*4	—	—	10	Number of frequency points in core of line (for Voigt line profiles only)
BANDWD	R*8	—	Doppler widths	4.	Total bandwidth for each line
BWCORE	R*8	—	Doppler widths	5.	Bandwidth of line cores
NANGLE	I*4	—	—	2	Number of angles
NCRAD	I*4	—	—	5	Number of impact parameter rays inside core (for spherical plasma with RADMIN > 0)

Variable Name	Type	Dimensions	Units	Default Value	Description
---------------	------	------------	-------	---------------	-------------

ION BEAM IONIZATION PARAMETERS

EBeam	R*8	MXZONS	MeV	0.	Beam energy
CURDEN	R*8	MXZONS	MA cm ⁻²	0.	Beam current density (i.e., particle flux in 10 ⁶ MA/s/cm ²)
IZBEAM	I*4	—	—	0	Beam atomic number
ISTGBM	I*4	—	—	0	Beam ionization state (1 \Rightarrow neutral)
ISW (37)	I*4	100	—	0	If > 0, consider ion impact ionization
PIMPIN	R*8	MXZONS, MXSUBS, MXSHEL, MXIONZ, MXGASS	transitions .sec ⁻¹ ·target ion ⁻¹	0.0	Ion beam impact ionization rate coefficient [For K _{α} calculations, the shell and subshell indices= 1.]

MULTIGROUP OPACITY PARAMETERS (Used for computing opacities for hydrodynamics codes)

NGRUPS	I*4	—	—	0	Number of photon energy groups
EGRPBD	R*8	MXGRPS+1	eV	0.0	Photon energy group boundaries

Variable Name	Type	Dimensions	Units	Default Value	Description
OTHER PARAMETERS					
CON	R*8	100	—	—	See Table 6.2
ISW	I*4	100	—	0	Array of constants (see Table 6.2)
IEDIT	I*4	100	—	0	Array of integer switches (see Table 6.3)
IBENCH	I*4	20	—	0	Array of edit (debugging) flags (see Table 6.4)
					Array used for benchmark test calculations
					IBENCH(3) = 1: 2-level atom with $\kappa \propto r^{-2}$
					2: 2-level atom with $\kappa \propto r^{-2}$ and $B_\nu \propto r^{-2}$
					(spherical case; see [38])
					IBENCH(4) = 1,2: 2-level atom (planar case; see [39])
					IBENCH(6) = 1: 2-level atom with continuum background (see [40])
CONVERGENCE PARAMETERS					
ERRMXF	R*8	—	—	—	1.e-3
IMAXSE	I*4	—	—	40	Maximum error allowed in fractional populations
CRSWCH	R*8	20	—	1.0	during convergence procedure
					Maximum number of iterations during convergence procedure
					Collisional-radiative switching parameters
					(used in subroutine STATEQ; see [41])
					(generally not needed for laboratory plasmas)
NGCYCL	I*4	—	—	4	Apply Ng acceleration every NGCYCL'th cycle
NGORDR	I*4	—	—	2	Order of Ng acceleration
NGBEGN	I*4	—	—	0	Iteration cycle at which to begin Ng acceleration

Table 6.2. Real Constants - CON

Array Element	Default Value	Description
6	1.e-30	Minimum value of fractional level population
12	0.1	Scaling parameter for statistical equilibrium matrix elements
19	1.e-7	Minimum fractional population used to test convergence
20	1.0	Multiplier for natural line width
21	1.0	Multiplier for Doppler line width
22	1.0	Multiplier for Stark line width
24	1.0	Multiplier for ion dynamic broadening (hydrogenic Lyman series)
25	0.0	Ratio of line-to-continuum opacity for benchmark calculation
26	1.0	Multiplier for bound-bound opacity
27	1.0	Multiplier for bound-free opacity
28	1.0	Multiplier for free-free opacity
42	1.0	Multiplier for collisional deexcitation rate
43	1.0	Multiplier for spontaneous emission rate
45	1.0	Multiplier for collisional recombination rate
46	1.0	Multiplier for radiative recombination rate
47	1.0	Multiplier for dielectronic recombination rate
48	1.0	Multiplier for autoionization rate
49	1.0	Multiplier for beam impact ionization rate
57	1.e-30	Minimum value of $\Delta E/T$ for ionization windowing
58	1.e-30	Minimum value of $\Delta E/T$ for ionization windowing

Table 6.3. Control Switches - ISW

Array Element	Value*	Description
4	0*	Compute radiative transfer (RT) for bound-free (b-f) transitions using escape probability model
	1	Compute RT for b-f transitions using multiangle, multifrequency Feautrier model
5	0*	Compute RT for bound-bound (b-b) transitions using escape probability model
	1	Compute RT for b-b transitions using multiangle, multifrequency Feautrier model
6	0	Start with coronal populations
	1*	Start with LTE populations
7	0*	Include photoexcitation effects in calculation of atomic level populations
8	0*	Include photoionization effects in calculation of atomic level populations
12	0*	Compute line radiation power densities (do not compute if nonzero)
14	0*	Neglect background continuum in escape probability line transport calculation
	1	Include background continuum
15	0*	Use automatic zoning procedure
	1	Specify grid by DRAD array in namelist input
17	0*	Use evenly spaced frequency grid in line core; logarithmically spaced grid in wings
	1	Use evenly spaced frequency grid for line transport calculation
18	0*	Use scaled values of source function and optical depth for photoionization calculation
	1	Use computed source functions and optical depths
20	0*	Non-LTE equation of state: $E = E_{\text{ion}} + E_e + E_{\text{iz}}$
	1	$E = E_{\text{ion}} + E_e + E_{\text{iz}} + E_{\text{degen}}$
	2	$E = E_{\text{ion}} + E_e + E_{\text{iz}} + E_{\text{DH}}$
	3	$E = E_{\text{ion}} + E_e + E_{\text{iz}} + E_{\text{degen}} + E_{\text{DH}}$
23	0*	Compute Voigt parameter
	1	Set Voigt parameter = CON (23)
	2	Estimate T and avoid from rate coefficients

An asterisk () indicates default value.

Table 6.3. (Continued)

Array Element	Value*	Description
30	0 1*	Compute \bar{g} in Stark width calculation Set $\bar{g} = 0.2$ in Stark width calculation
34	0* 1	Use LAPACK matrix scaling Use LAPACK + NLTERT matrix scaling
36	0* 1	Set up Auger rates for inner-shell transitions Do not set up arrays for Auger rates
37	0* 1 2 3	Neglect effect of ion beam on populations Use old ion impact ionization model Use term-dependent ion impact ionization cross sections Use term-dependent cross sections, Auger rates, and fluorescence yields
38	0* 1	No equation of state calculation Compute internal energy and pressure
39	0* 1	No multigroup opacity calculation Compute multigroup opacities
44	0* 1	Use $T(r)$, $n(r)$ from namelist input Use $T(r)$, $n(r)$ from hydro output
45	0*	Parameter to indicate hydro simulation time for setting $T(r)$, $n(r)$
87	0*	Parameter used in 2-level atom benchmark calculations

An asterisk () indicates default value.

Table 6.4. Debugging Switches - IEDIT

<u>Array Element</u>	<u>Subroutine Writing Debug Output</u>
18	CPLC1P
18	CPLC9P
18	CPLCFP
84	FESCAP
10	FORM1C
9	FORM1L
10	FORM3C
9	FORM3L
12	GETCFS
78	GPOPAC
48	IIXSEC
44	INIT2
28,29	INPUT
71	INPUT4
72	INPUT5
61	LINEPR
80	LINWID
11,27	LOPACS
1,14,54	MATRX0
52	MESHHV
77	MESHMG
78	MGOPAC
34	NGACCL
59	OUT3
25	PWRDEN
42	RATBEM
41	RATCOF
47,81	READA2
12,55	RRATES
82,83,85,86	SPECT1
85	SPECT2
85	SPECT3
6,15	STATEQ
92	VOIGT
81	WSTARK

7. Subroutines

Table 7.1 lists the name of each subroutine in NLTERT along with a brief description of its primary function. A flow diagram showing the relation of the higher level subroutines is shown in Fig. 7.1. With the exception of using NAMELIST input, all subroutines are written in FORTRAN 77.

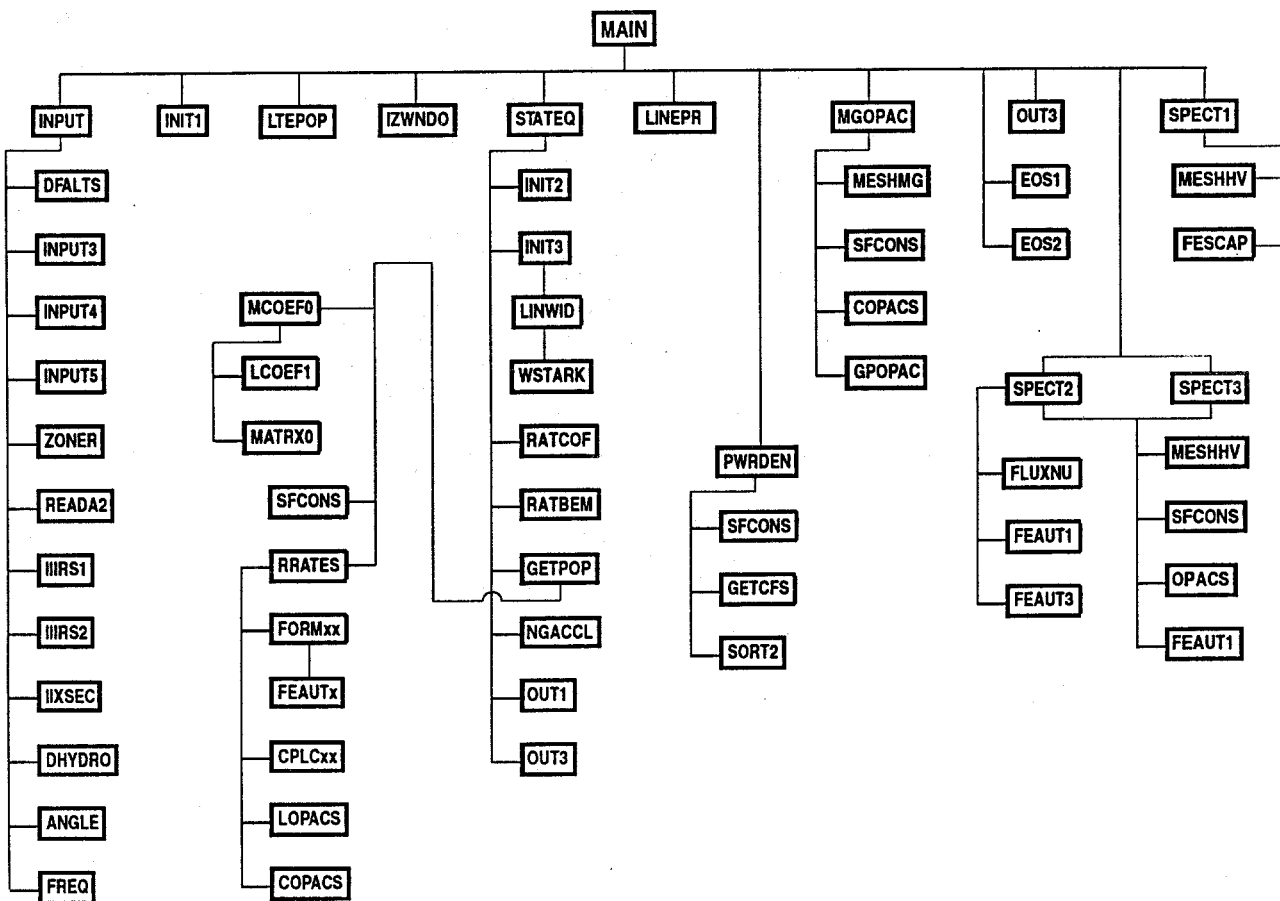


Figure 7.1. Flow diagram for selected subroutines in NLTERT.

Table 7.1. NLTERT Subroutines

Subroutine Name	Called By	Calls To	Description
MAIN	—	INPUT, INIT1, IZWENDO, LTEPOP, PWRDEN, LINEPR, SPECT1, SPECT2, SPECT3, MGOPAC, STATEQ, OUT3	Driver routine (main program).
BDATA	—	—	Block data routine for initializing constants.
ANGLE	INPUT	—	Sets up angles and integration weights for radiative transfer calculation.
AVG	WSTARK	EXTROP, YVALUE	Computes effective Gaunt factors for Stark broadening.
BFARGS	CPLCFS, CPLCFP, CPLCF9	—	Sets up bound-free escape probability parameters.
COPACS	FORM1C, FORM3C, GETCFS, MGOPAC, RRATES	—	Computes frequency-dependent continuum opacities and emissivities.
CPLC1P	RRATES, GETCFS	EPINT1	Computes escape probability coupling coefficients for Doppler profiles in planar geometry.
CPLC9P	RRATES, GETCFS	EPINT9, BFARGS	Computes escape probability coupling coefficients for bound-free transitions in planar geometry.
CPLCFP	RRATES, GETCFS	EPINT2, EPINT3, BFARGS	Computes escape probability coupling coefficients for bound-bound transitions in planar geometry.
CPLCFS	RRATES, GETCFS	EPINT1, EPINT2, EPINT3, EPINT9, BFARGS	Compute escape probability coupling coefficients for bound-bound transitions in cylindrical and spherical geometry.
DFALTS	INPUT	—	Initialize variables and set default values.
DHYDRO	INPUT	DTABLE, FNEWT	Set up temperature and density distributions from hydrodynamics simulation output.
DTABLE	DHYDRO	—	Sets up divided difference tables for interpolation.
ECOUMB	EOS1	FERMID	Calculates Debye-Hückel correction term to the plasma internal energy.

Table 7.1 (Continued)

Subroutine Name	Called By	Calls To	Description
EITA	EOS1, EOS2	FERMID	Determines degeneracy factor for a partially degenerate electron gas.
EOS1	MAIN	FERMID, ECOUMB, EITA	Computes plasma internal energy.
EOS2	MAIN	FERMID, PCOUMB, EITA	Computes plasma pressure.
EPINT1	CPLC1P, CPLCFS	—	Computes escape probability integral for a Doppler profile.
EPINT2	CPLCFP, CPLCFS	—	Computes escape probability integral for a Lorentz profile.
EPINT3	CPLCFP, CPLCFS	—	Compute escape probability integral for a Voigt profile.
EPINT9	CPLC9P, CPLCFS	—	Compute escape probability integral for bound-free transitions.
FEAUT1	FLUXNU, SPECT2, SPECT3	—	Feautrier radiative transfer algorithm for planar geometry (spectral calculation).
FEAUT3	FLUXNU	—	Feautrier radiative transfer algorithm for spherical geometry (spectral calculation).
FEAUTP	FORMIC, FORMIL	—	Feautrier radiative transfer algorithm for planar geometry.
FEAUTX	FORMIC, FORMIL	—	Feautrier radiative transfer algorithm for spherical geometry.
FERMID	ECOUMB, EITA, EOS1, EOS2, PCOUMB	—	Computes Fermi-Dirac integrals.
FESCAP	SPECT1	—	Calculates escape probability factors.
FLUXNU	SPECT2	FEAUT1, FEAUT3	Computes frequency-dependent flux using Feautrier radiative transfer model.
FNEWT	DHYDRO	—	Newton divided difference interpolation routine.

Table 7.1 (Continued)

Subroutine Name	Called By	Calls To	Description
FORM1C	GETCFS, RRATES	COPACS, FEAUTP	Solves formal solution of transfer equation to obtain photoionization rate in planar geometry.
FORM1L	GETCFS, RRATES	VOIGT, FEAUTP	Solves formal solution of transfer equation to obtain photoexcitation rate in planar geometry.
FORMBC	GETCFS, RRATES	COPACS, FEAUTX	Solves formal solution of transfer equation to obtain photoionization rate in spherical geometry.
FORMBL	GETCFS, RRATES	VOIGT, FEAUTX	Solves formal solution of transfer equation to obtain photoexcitation rate in spherical geometry.
FREQ	INPUT	—	Sets of frequency mesh and integration weights for bound-bound transitions.
GETCFS	PWRDEN	FORM1C, FORM1L, FORM3C, FORM3L, CPLC1P, CPLC9P, CPLCFP, CPLCFS, COPACS, LOPACS	Compute zone-to-zone coupling coefficients for all transitions.
GETPOP	STATEQ	MCOEF0, RRATES, SFCONS	Computes atomic level populations for all gas species.
GINT5	GPOPAC	—	Computes integrals used for evaluation of Planck opacities.
GINT6	GPOPAC	—	Computes integrals used for evaluation of Rosseland opacities.
GPOPAC	MGOPAC	GINT5, GINT6	Computes Planck and Rosseland opacities for a single group.
HIRS1	INPUT	—	Sets up ion impact ionization cross sections, fluorescence yields, and Auger rates for Al and Au.
HIRS2	INPUT	—	Sets up ion impact ionization cross sections, fluorescence yields, and Auger rates for Al.

Table 7.1 (Continued)

Subroutine Name	Called By	Calls To	Description
IIXSEC	INPUT	—	Computes ion impact ionization rate coefficients as a function of ion beam parameters.
INIT1	MAIN	—	Initialize some atomic parameters and print out control switches and constants.
INIT2	STATEQ	—	Initialize radiative transfer parameters.
INIT3	STATEQ	LINWID	Initialize line profile parameters.
INPUT	MAIN	INPUT3, INPUT4, INPUT5 ZONER, (DATE,) IIIRS1, IIIRS2, READA2, IIXSEC, FREQ, DFALTS, ANGLE, DHYDRO NSHELL	Input controller routine. Reads in photoionization data.
INPUT4	INPUT	—	Reads in ion beam impact ionization cross sections.
INPUT5	INPUT	—	Reads in Auger rates, fluorescence yields, and ion beam impact ionization cross sections.
IZWNDO	MAIN	—	Sets range of ionization stages to be considered for each spatial zone.
LCOEFL	MCOEFL	—	Sets up statistical equilibrium matrix coefficients.
LINEPR	MAIN	VOIGT	Computes line profile parameters.
LINWID	RRATES	WSTARKE, OCWITH	Sets up line broadening parameters.
LOPACS	GETCFS, RRATES	VOIGT	Computes source functions and opacities for a given line.
LTEPOP	MAIN	—	Computes LTE populations for each zone.
MATRX0	MCOEFL	LAPACK routines	Inverts statistical equilibrium matrix to get atomic level populations for 1 spatial zone.
MCOEFL	GETPOP	LCOEFL1, MATRX0	Sets up and solves statistical equilibrium equations for all zones.
MESHHV	SPECT1, SPECT2, SPECT3	SORT	Sets up photon energy grid for spectral calculations.

Table 7.1 (Continued)

Subroutine Name	Called By	Calls To	Description
MESHMG	MGOPAC	SORT	Sets up photon energy groups for multigroup opacity calculations.
MGOPAC	MAIN	MESHMG, SFCONS, COPACS, GPOPAC	Computes Planck and Rosseland multigroup opacities.
NGACCL	STATEQ	SIMUL	Ng acceleration algorithm.
NSHELL	INPUT3	—	Finds the number of subshells in an atomic configuration.
OCWITH	LINWID	—	Sets up line broadening parameters for H-like ions at high density.
OPACS	SPECT2, SPECT3	VOIGT	Computes total source function and opacity at each spatial point.
OUT1	STATEQ	—	Prints out population distributions.
OUT3	MAIN, STATEQ	—	Prints out transition rates.
PCOUMB	EOS2	—	Calculates Debye-Hückel correction term to plasma pressure.
PWRDEN	MAIN	SFCONS, GETCFS, SORT2	Computes line and bound-free power densities for radiation escaping the plasma.
RATBEM	STATEQ	—	Calculates ion beam impact ionization rate coefficients.
RATCOF	STATEQ	—	Calculates collisional and radiative rate coefficients.
READA2	INPUT	—	Reads in atomic data.
RRATES	GETPOP	FORM1C, FORM1I, FORM3C, FORM3L, CPLCIP, CPLC9P, CPLCFP, CPLCFS, COPACS, LOPACS, VOIGT, LINEPR	Computes radiation-dependent rate coefficients.
SFCONS	MGOPAC, PWRDEN	— SPECT2, SPECT3	Sets up parameters for source function calculations.
SIMUL	NGACCL	—	Solves a set of linear equations (for small matrices only).

Table 7.1 (Continued)

Subroutine Name	Called By	Calls To	Description
SORT	MESHHV, MESHMG	—	Sorting algorithm.
SORT2	PWRDEN	—	Sorting algorithm.
SPECT1	MAIN	VOIGT, MESHHV, FESCAP	Computes spectrum using escape probability radiative transfer model.
SPECT2	MAIN	MESHHV, SFCONS, OPACS, FLUXNU, FEAUT1	Computes spectrum using multiangle, multifrequency radiative transfer model.
SPECT3	MAIN	MESHHV, SFCONS, OPACS, FEAUT1	Computes emission spectrum along specified line of sight.
STATEQ	MAIN	INTT2, INIT3, RATCOF, RATBEM, GETPOP, NGACCL, OUT1, OUT3	Determines distribution of atomic populations from self-consistent solution of statistical equilibrium equations and radiation field.
VOIGT	FORM1L, FORM3L, LINEPR, LOPACS, OPACS, SPECT1	—	Compute Voigt line profile.
WSTARK	LINWID	AVG	Computes Stark width for a given line.
YVALUE	AVG	Several internal routines	Routines used to compute Gaunt factors for Stark broadening.
ZONER	INPUT	—	Sets up spatial zoning.

8. Common Blocks

Listed in Table 8.1 are the common blocks used in NLTERT. For each common block, the variable name, type, dimensions, and a brief description of each variable is provided. In most cases, the dimensions of variables are specified by quantities defined in parameter statements. These parameters are:

Parameter	Description
MXLVLS	Maximum number of atomic levels
MXTRNS	Maximum number of atomic transitions
MXGASS	Maximum number of gas species
MXIONZ	Maximum number of ionization stages (per gas species)
MXLVLI	Maximum number of levels in atomic data file
MXPHOT	Maximum number of frequency points in spectral calculation
MXZONS	Maximum number of spatial zones
MXDATT	Maximum number of temperatures in rate coefficient tables
MXDATD	Maximum number of electron densities in rate coefficient tables
MXDATE	Maximum number of beam energies in ion impact cross section table
MXANGL	Maximum number of angles in radiative transfer calculation
MXFREQ	Maximum number of frequency points per line
MXIMPS	Maximum number of impact parameter rays in spherical radiative transfer calculation
MXSSHLL	Maximum number of atomic subshells
MXGRPS	Maximum number of groups for multigroup opacity calculation.

Table 8.1. Common Blocks
COMMON/ATDATA/

Variable	Type	Dimensions	Units	Description
TEMIN	R*8	MXGASS	eV	Minimum electron temperature for rate coefficient grid
DLOGTE	R*8	MXGASS	—	Logarithmic increment (base 10) of electron temperature for rate coefficient grid
DEMIN	R*8	MXGASS	cm ⁻³	Minimum electron density for rate coefficient grid
DLOGDE	R*8	MXGASS	—	Logarithmic increment (base 10) of electron density for rate coefficient grid
CLDEXA	R*4	MXDATT, MXTRNS	cm ³ s ⁻¹	Collision excitation rate coefficient due to thermalized electrons
SPNEMA	R*8	MXTRNS	s ⁻¹	Spontaneous emission rate
CLRECA	R*4	MXDATT, MXTRNS	cm ⁶ s ⁻¹	Collisional recombination rate coefficient due to thermalized electrons
RDRECA	R*4	MXDATT, MXTRNS	cm ³ s ⁻¹	Radiative recombination rate coefficient
DIELRA	R*4	MXDATT, MXDATD, MXTRNS	cm ³ s ⁻¹	Dielectronic recombination rate coefficient
AUTIZA	R*4	MXTRNS	s ⁻¹	Autoionization rate coefficient
PMPIZA	R*4	MXZONS, MXTRNS	s ⁻¹	Ion beam impact ionization rate coefficient
FLOYLD	R*8	MXLVLS	—	Fluorescence yield
NDATTE	I*4	MXGASS	—	Number of points in temperature grid of atomic data file
NDATDE	I*4	MXGASS	—	Number of points in electron density grid of atomic data file

Values for the above variables are read in from ATBASE files and stored. The exception to this is PMPIZA, which is computed when the old proton impact ionization model is used.

COMMON/ATOMIC/

Variable	Type	Dimensions	Units	Description
ATOMWT	R*8	MXGASS	amu	Atomic weight
FRACSP	R*8	MXZONS, MXGASS	—	Fractional abundance (by number density) of each gas species
STATWT	R*8	MXLVLS	—	Statistical weight
ENERGY	R*8	MXLVLS	eV	Atomic level energy measured relative to fully ionized
EREFER	R*8	MXGASS	eV	Reference energy for equation of state calculation
ENBIND	R*8	MXLVLS,	a.u.	Electron binding energy used for Stark width calculation
STRKR2	R*8	MXSHEL, MXLVLS, MXSHEL (= a_0)	a.u. (= a_0)	Electron mean squared orbital radius for Stark width calculation
STRKDE	R*8	MXLVLS	a.u.	Energy to nearest level for Stark width calculation
STARKF	R*8	MXLVLS	—	Gaunt factor parameter for Stark width calculation
STKRI	R*8	MXLVLS	a.u.	Orbital radius of level of interest for Stark width calculation
STKRIP	R*8	MXLVLS	a.u.	Orbital radius of nearest level for Stark width calculation
NLEVLS	I*4	—	—	Total number of atomic levels
IONSTG	I*4	MXLVLS	—	Ionization stage ($1 \Rightarrow$ neutral)
IGROUN	I*4	MXGASS, MXIONZ	—	Level index of ground state for each ion
NGASES	I*4	—	—	Number of gas species

COMMON/ATOMIC/ (Continued)

Variable	Type	Dimensions	Units	Description
LKMIN	I*4	MXGASS	—	Index of first (lowest) energy level for each gas species
LKMAX	I*4	MXGASS	—	Index of last (highest) energy level for each gas species
NLEVLK	I*4	MXGASS	—	Number of energy levels for each gas species
LKJMIN	I*4	MXGASS	—	Index for first (lowest) energy level for each ion
LKJMAX	I*4	MXIONZ, MXGASS, MXIONZ	—	Index of last (highest) energy level for each ion
IZGAS	I*4	MXGASS, MXVLS	—	Atomic number of each gas
KGAS	I*4	MXVLS	—	Gas species index
LMINZN	I*4	MXZONS, MXGASS	—	Index of lowest energy level for each gas in each zone
LMAXZN	I*4	MXZONS, MXGASS	—	Index of highest energy level for each gas in each zone
NLEVZN	I*4	MXZONS, MXGASS	—	Index of energy levels for each gas in each zone

COMMON/ATRANS/

Variable	Type	Dimensions	Units	Description
ETRANS	R*8	MXTRNS	eV	Transition energy
OSCSTR	R*8	MXTRNS	—	Oscillator strength
PROFLC	R*8	MXZONS, MXTRNS	Hz ⁻¹	Value of line profile at line center ($\int \phi_\nu d\nu = 1$)
AVOIGT	R*8	MXZONS, MXTRNS	—	Voigt profile damping parameter
TAUTOT	R*8	MXTRNS	—	Total optical depth for each transition
WIDNAT	R*8	MXTRNS	eV	Natural line width
WIDDOP	R*8	MXTRNS	eV ^{3/2}	Doppler line width
WIDSTK	R*8	MXZONS, MXTRNS	eV ^{3/2} cm ³	Stark line width
WIDION	R*8	MXZONS, MXTRNS	eV	Stark ion dynamic broadening
ILINEP	I*4	—	—	Line profile type (1 \Rightarrow Doppler; 2 \Rightarrow Lorentz; 3 \Rightarrow Voigt)
ITTYPE	I*4	MXTRNS	—	Transition type (1 \Rightarrow bound-bound; 6-10 \Rightarrow bound-free)
LUPPER	I*4	MXTRNS	—	Upper level index of transition
LLOWER	I*4	MXTRNS	—	Lower level index of transition
NTRANS	I*4	—	—	Total number of transitions
MINTRN	I*4	MXGASS	—	Minimum transition index of gas
MAXTRN	I*4	MXGASS	—	Maximum transition index of gas
MXIZCH	I*4	—	—	Maximum change in ionization state considered for bound-free transitions
LTRANS	I*2	MXLVLS, MXLVLS	—	Transition index for (upper, lower) levels

COMMON/CLOCAL/

Variable	Type	Dimensions	Units	Description
AMATF	R*8	MXLVLS+1, MXLVLS+1	—	Coefficients for statistical equilibrium matrix
COMMON/CMATRIX/				
AMAT1	R*8	MXLVLS+1, MXLVLS+1	—	Coefficients for statistical equilibrium matrix
COMMON/CONSTS/				
HPLANK	R*8	—	eV s	Planck's constant
BOLTZK	R*8	—	—	Boltzmann's constant
CLIGHT	R*8	—	cm s ⁻¹	Speed of light
AMUMAS	R*8	—	g	Atomic mass unit
RYDBRG	R*8	—	eV	Rydberg (= 13.6 eV)
AVGDR0	R*8	—	—	Avogadro's number
ZERO	R*8	—	—	Zero
ONE	R*8	—	—	One
TWO	R*8	—	—	Two
HALF	R*8	—	—	One-half
THIRD	R*8	—	—	One-third
SIXTH	R*8	—	—	One-sixth
PI	R*8	—	—	π
FOURPI	R*8	—	—	4π
SQRTPI	R*8	—	—	$\pi^{1/2}$
SPIINV	R*8	—	—	$\pi^{-1/2}$

COMMON/CONTRL/

Variable	Type	Dimensions	Units	Description
CON	R*8	100	—	Array of constants (see Table 6.2)
XMUBAR	R*8	—	—	Mean cosine angle for escape probability model
XMULOS	R*8	—	—	Cosine angle of line-of-sight for emergent flux calculation
ERRMXF	R*8	—	—	Maximum fractional error in atomic level populations
CRSWCH	R*8	20	—	Collisional-radiative switching parameter
RATMIN	R*8	—	—	Minimum value for rate coefficients (≈ 0)
NGCYCL	I*4	—	—	Apply Ng acceleration every NGCYCL'th cycle
NGORDR	I*4	—	—	Order of Ng acceleration
NGBEGN	I*4	—	—	Iteration cycle to begin Ng acceleration
ISW	I*4	100	—	Array of switches (see Table 6.3)
IPLOT	I*4	30	—	Array of switches (see Section 6)
IEDIT	I*4	100	—	Array of debug switches (see Table 6.4)
IMAXSE	I*4	—	—	Maximum number of iterations for statistical equilibrium cycle
IREADA	I*4	MXGASS	—	Switch for reading formatted atomic data files
IBENCH	I*4	20	—	Switch for benchmarking calculations

COMMON/FILUNS/

LUN	I*4	100	—	Logical unit numbers of input and output files
FNAMES	C*16	100	—	File names of input and output files

COMMON/GRID/

Variable	Type	Dimensions	Units*	Description
RADIUS	R*8	MXZONS+1	cm	Spatial zone boundaries
DRAD	R*8	MXZONS	cm	Zone width
RBAR	R*8	MXZONS	cm	Position of zone midpoint
DRAY	R*8	MXZONS	—	Parameters used in escape probability model
DDRAY	R*8	MXZONS,	—	Parameters used in escape probability model
DRAYS	R*8	MXZONS,	—	Parameters used in escape probability model
DDRAYS	R*8	MXZONS,	—	Parameters used in escape probability model
XNEONA	R*8	MXZONS,	—	Ratio of number of atoms in emitting zone to that in absorbing zone
VOLZON	R*8	MXZONS	cm ^α	Volume in each spatial zone
VOLTOT	R*8	—	cm ^α	Total volume of plasma
GEOMA	R*8	3	—	(1,2π,4π) for IGEOM = (1,2,3)
GEOMV	R*8	3	—	(1,π,4π/3) for IGEOM = (1,2,3)
DELROZ	R*8	MXZONS,	—	(Δr/Δz) for spherical radiative transfer calculation
MXIMPS	MXIMPS	—	—	
BMURAD	R*8	MXZONS+1,	—	Cosine angle for flux calculation
WTINT0	R*8	MXIMPS,	—	Angle integration weights for mean intensity calculation
WTFLX0	R*8	MXIMPS,	—	Angle integration weights for flux calculation
		MXZONS+1	—	

COMMON/GRID/ (Continued)

Variable	Type	Dimensions	Units*	Description
NZONES	I*4	—	—	Number of spatial zones
IGEOM	I*4	—	—	Geometry index*
KMINCP	I*4	MXZONS	—	Zone indexing parameters for coupling coefficient calculation
NCRAD	I*4	—	—	Number of impact parameters within “core”
NDRAD	I*4	—	—	Number of impact parameters outside “core” (= NZONES+1)
NPRAD	I*4	—	—	Total number of impact parameters (for spherical RT calculation)
NIRAD	I*4	MXIMPS	—	Number of points along each impact parameter

$$^*\alpha = \text{IGEOM} = \begin{cases} 1 & \text{planar} \\ 2 & \text{cylindrical} \\ 3 & \text{spherical} \end{cases}$$

COMMON/GRIDF/

Variable	Type	Dimensions	Units	Description
XFREQ	R*8	MXFREQ	—	Frequency mesh for line transport calculation (in Doppler widths)
WTFREQ	R*8	MXFREQ	—	Weights for frequency integration
WTANGL	R*8	MXANGL	—	Weights for angle integration
XMU	R*8	MXANGL	—	Angle mesh for radiative transfer calculation
NFLINE	I*4	—	—	Number of frequency points for line transport calculation
NFCORE	I*4	—	—	Number of frequency points in line “core” of Voigt profile
NFPIZO	I*4	—	—	Number of frequency points for photoionization rate calculation
NANGLE	I*4	—	—	Number of angle points for radiative transfer calculation

COMMON/IBEAM/

Variable	Type	Dimensions	Units	Description
EBeam	R*8	MXZONS	MeV	Ion beam energy (velocity)
CURDEN	R*8	MXZONS	MA cm ⁻²	Ion beam current density
BIXSEC	R*4	MXDATE, MXTRNS	cm ²	Beam impact ionization cross section
EBMMIN	R*8	MXGASS	MeV	Minimum beam energy for beam ionization cross section grid
DLOGEB	R*8	MXGASS	—	Logarithmic increment (base 10) of beam energy for cross section grid
IZBEAM	I*4	—	—	Beam atomic number
ISTGBM	I*4	—	—	Beam ionization stage (1 \Rightarrow neutral)
NDATEB	I*4	MXGASS	—	Number of beam energy points in beam ionization cross section grid

COMMON/OPACMG/

EGRPPBD	R*8	MXGRPS+1	eV	Photon energy group boundaries for multigroup opacity calculation
NGRUPS	I*4	—	—	Number of photon energy groups

COMMON/PIXSEC/

HVEDGE	R*8	MXTRNS	eV	Energy of photoionization edge ($h\nu_1$)
PIXS0	R*8	MXTRNS	cm ²	Photoionization cross section at threshold
PIBETA	R*8	MXTRNS	—	“ β ” in cross section fit*
PISEXP	R*8	MXTRNS	—	“ s ” in cross section fit*
MNHVPI	I*4	MXTRNS	—	Minimum photon energy index such that $\nu \geq \nu_1$

*Photoionization cross sections are fit to:

$$\alpha(\nu) = \alpha(\nu_1) \left\{ \beta \left(\frac{\nu_1}{\nu} \right)^s + (1 - \beta) \left(\frac{\nu_1}{\nu} \right)^{s+1} \right\}, \quad \nu \geq \nu_1.$$

COMMON/POPULS/					
Variable	Type	Dimensions	Units	Description	
POPSAV	R*4	MXLVLS, MXZONS,	—	Saved values of fractional level populations from previous (up to 6) iterations	6
COMMON/RADCFSS/					
CCCFSS	R*8	MXZONS, MXTRNS	—	“Residual” of Λ -operator	
CCFS1	R*8	MXZONS, MXTRNS	—	“Diagonal” of Λ -operator	
COMMON/RADTRN/					
CCOEFS	R*8	MXZONS, MXZONS	—	Zone-to-zone coupling coefficients	
TAU	R*8	MXZONS+1	—	Optical depth integrated from plasma surface	
DTAU	R*8	MXZONS	—	Optical depth for each zone	
COMMON/RATCFSS/					
COLEXC	R*8	MXZONS, MXTRNS	cm ³ s ⁻¹	Collisional excitation rate coefficient	
COLDEX	R*8	MXZONS, MXTRNS	cm ³ s ⁻¹	Collisional deexcitation rate coefficient	
COLLIZ	R*8	MXZONS, MXTRNS	cm ³ s ⁻¹	Collisional ionization rate coefficient	

COMMON/RATCFS/

Variable	Type	Dimensions	Units	Description
COLREC	R*8	MXZONS, MXTRNS	cm ⁶ s ⁻¹	Collisional recombination rate coefficient
RADREC	R*8	MXZONS, MXTRNS	cm ³ s ⁻¹	Radiative recombination rate coefficient
DIELRC	R*8	MXZONS, MXTRNS	cm ³ s ⁻¹	Dielectric recombination rate coefficient
AUTOIZ	R*8	MXTRNS, MXZONS, MXTRNS	s ⁻¹	Autoionization rate
PIMPIZ	R*8	MXZONS, MXTRNS	s ⁻¹	Proton impact ionization rate
BIMPIZ	R*8	MXZONS, MXTRNS	s ⁻¹	Ion beam impact ionization rate
SPONEM	R*8	MXTRNS	s ⁻¹	Spontaneous emission rate
COMMON/SFNCON/				
CONBFA	R*8	MXZONS, MXTRNS	cm ⁻³	Bound-free absorption constant
CONBFE	R*8	MXZONS, MXTRNS	eV ⁻² cm ⁻⁵	Bound-free emission constant
CONBBA	R*8	MXZONS, MXTRNS	cm ⁻¹ s ⁻¹	Bound-bound absorption constant
CONBBE	R*8	MXZONS, MXTRNS	eV ⁻² cm ⁻³ s ⁻¹	Bound-bound emission constant
FFCONA	R*8	MXZONS	cm ⁻¹	Free-free absorption constant
FFCONE	R*8	MXZONS	eV ⁻² cm ⁻³	Free-free emission constant
CONLTE	R*8	MXZONS	—	Bound-free constant

COMMON/SPECTR/

Variable	Type	Dimensions	Units	Description
HVMIN	R*8	—	eV	Minimum photon energy of spectral calculation
HVMAX	R*8	—	eV	Maximum photon energy of spectral calculation
NFRQFF	I*4	—	—	Number of continuum photon energy points in spectral grid
NFRQBB	I*4	—	—	Number of photon energy points per bound-bound transition

COMMON/STRING/

CONFIG	C*130	MXLVLS	—	Atomic configuration
TRMSYM	C*10	MXLVLS	—	Atomic term symbol

COMMON/THERMO/

TEMPEL	R*8	MXZONS	eV	Electron temperature
TMPION	R*8	MXZONS	eV	Ion temperature
DENSNN	R*8	MXZONS	cm ⁻³	Ion number density
DENSNE	R*8	MXZONS	cm ⁻³	Electron density

9. Sample Calculations

9.1. Example 1: Thermal Spectrum for Aluminum

The first example is for a planar Al plasma with an ion density of $n = 10^{20} \text{ cm}^{-3}$, a temperature of $T = 30 \text{ eV}$, and a slab width of 0.012 cm. This corresponds to a $0.2 \mu\text{m}$ -thick solid density foil which has expanded by a factor of 600. Under these conditions, the plasma populations are close to LTE (within about a factor of 2), but the plasma is not thick enough for the spectrum to be that of a blackbody. (If the plasma were optically thick ($\tau_\nu \gg 1$) at all frequencies the spectrum of an LTE plasma would be a blackbody spectrum.) The input file is shown in Fig. 9.1, while the calculated emission spectrum is shown in Fig. 9.2. The frequency-dependence of the optical depth is shown in Fig. 9.3.

9.2. Example 2: 2-Level Atom

Figure 9.4 shows the input file for a 2-level atom calculation in spherical geometry. The bound-bound transition corresponds to the Ly α line of Al ($h\nu = 1.728 \text{ keV}$). The plasma temperature, density, and radius were chosen to give a value of the scattering (or “quenching”) parameter of $\varepsilon = 10^{-4}$ and line center optical depth of 5.64×10^3 . The line is specified to have a Doppler profile. The multifrequency radiative transfer model is used in this case (ISW(5) = 1). The number of spatial grid points is 20.

The spatial distribution of the source function is shown in Fig. 9.5 for 2 cases: $\tau_{\max} = 5.64 \times 10^3$ and 56.4. The results are in good agreement with previously published calculations [38].

9.3. Example 3: K $_\alpha$ Absorption Spectrum for Aluminum

The input file for calculation of an Al K $_\alpha$ absorption spectrum is shown in Fig. 9.6. The plasma conditions are: $T = 58 \text{ eV}$, $\rho = 0.02 \text{ g/cm}^3$, and the plasma thickness is $6.75 \mu\text{m}$ (which correspond to a 500 Å foil which has expanded by a factor of 135). The atomic level populations are calculated in the LTE approximation (ISW(6) = 3). The calculated absorption spectrum (transmission $\equiv \exp(-\tau_\nu)$) is shown in Fig. 9.7. Results from calculations of this type are in good agreement with experimental data for laser-produced plasmas [7].

```

$input1
c ...
    iplot(1) = 1
    iplot(8) = 1, 1,
c ...
    hvmin = 1.
    hvmax = 1000.
    nfrqbb = 5
    nfrqff = 1000
c ...
    xmulos = .51
c ...
    isw(36) = 1
c ...

    igeom = 1
    nzones = 6
    radmin = 0.
    radmax = 1.2e-2
    dradmn = 1.2e-4
c ...
    tempel(1) = 6*30.,
    densnn(1) = 6*1.e20
c ...
    atomnm = 13.
    atomwt = 27.0
    ilinep = 3
c ...
c ...
c ...   thermal states
c ...
c ...   -----
c Al I      iselct( 1,1) = 4*0
c Al II     iselct( 11,1) = 16*0
c Al III    iselct( 34,1) = 3*0
c Al IV     Ne-like
            iselct(133,1) = 10*1
c Al V      F-like
            iselct(243,1) = 20*1
c Al VI     O-like
            iselct(402,1) = 20*1
c Al VII    N-like
            iselct(614,1) = 50*1
c Al VIII   C-like
            iselct(791,1) = 37*1
c Al IX     B-like
            iselct(949,1) = 24*1
c Al X      Be-like
            iselct(1046,1) = 27*1
c Al XI     Li-like
            iselct(1149,1) = 11*1
c Al XII    He-like
            iselct(1228,1) = 20*1
c Al XIII   H-like
            iselct(1256,1) = 3*1
c Al XIV    Fully Ionized
            iselct(1266,1) = 1
$end

```

PLOTTING SWITCHES

SPECTRAL GRID PARAMETERS (energies in eV)

MEAN DIFFUSIVITY ANGLE FOR SPECTRAL CALCULATION

do NOT read in Auger rates if isw36 <> 0

SPATIAL GRID INFO

grid temperatures and ion densities

ATOMIC DATA PARAMETERS

SELECT LEVELS

Figure 9.1. Namelist input for Example 1.

Aluminum Emission Spectrum
 $T = 30 \text{ eV}$, $n = 10^{20} \text{ cm}^{-3}$, $L_{\text{orig}} = 0.2 \mu\text{m}$

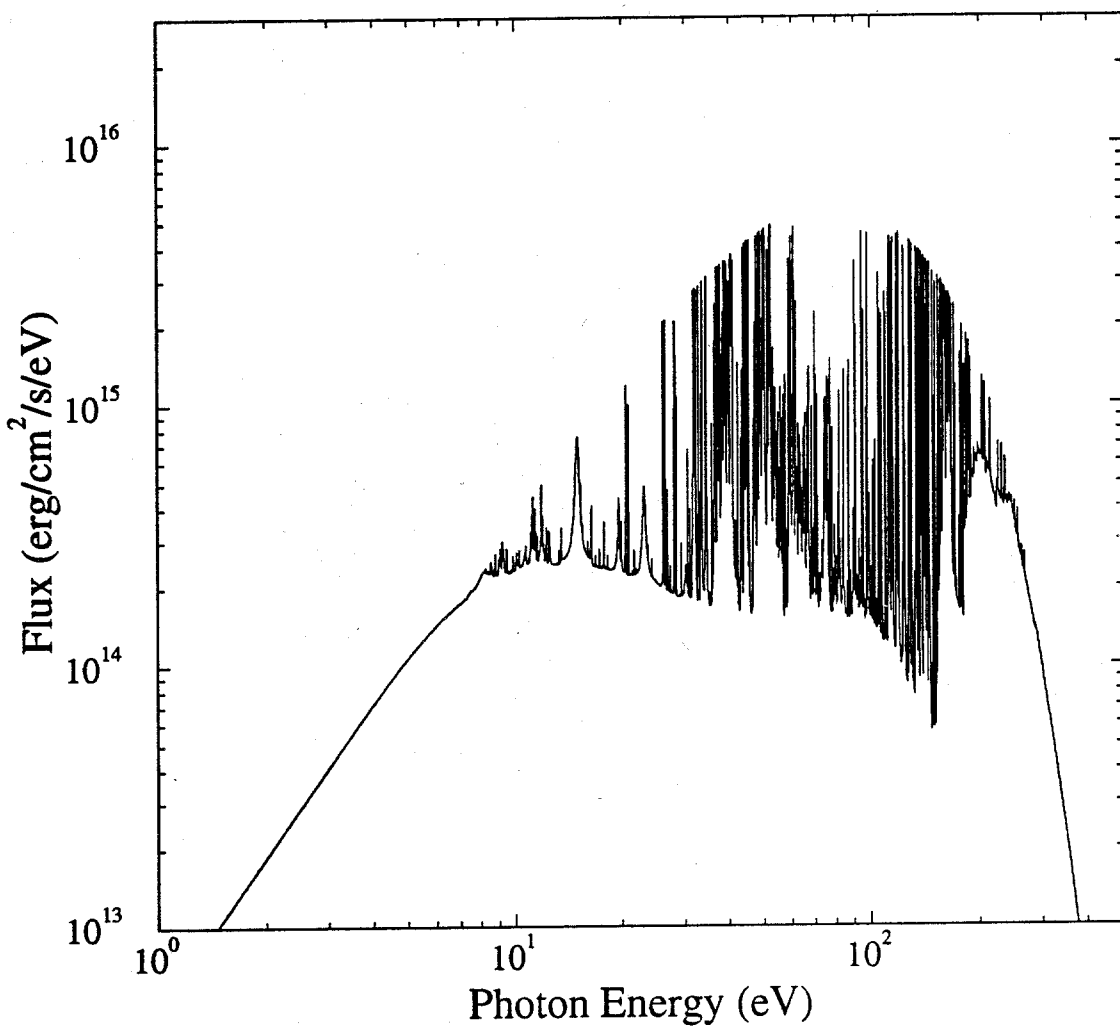


Figure 9.2. Emission spectrum for Example 1.

Aluminum Optical Depth vs. Frequency
 $T = 30 \text{ eV}$, $n = 10^{20} \text{ cm}^{-3}$, $L_{\text{orig}} = 0.2 \mu\text{m}$

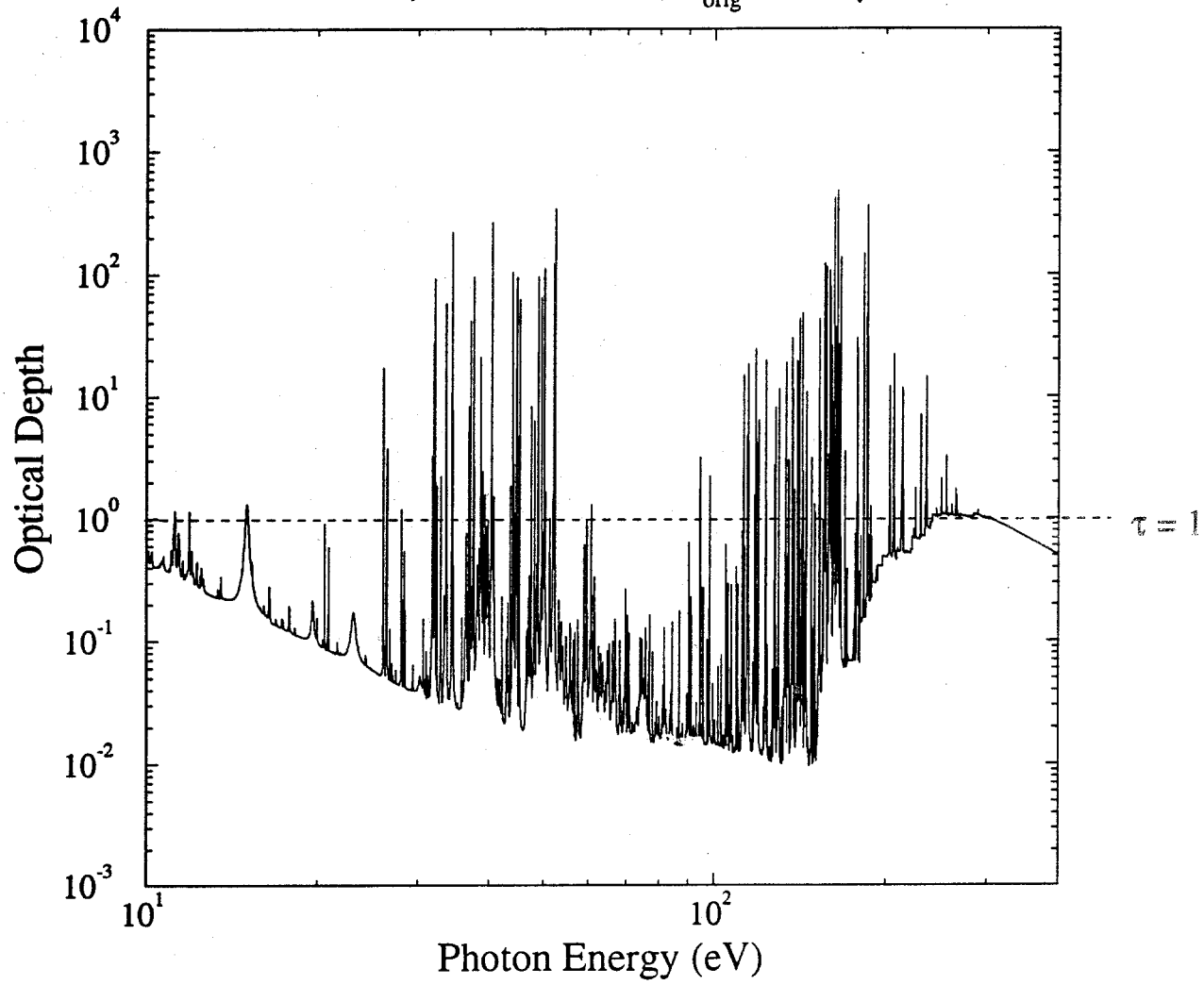


Figure 9.3. Frequency-dependent optical depths for Example 1.

```

$input1
c ...
    isw(5) = 1
c ...
c
c
c
    isw(6) = 1
c ...
    isw(36) = 1
c ...
    iplot(1) = 3
    iplot(2) = 1
    iplot(8) = 1, 1,
c ...
    hvmin = 1720.
    hvmax = 1730.
    nfrqbb = 7
    nfrqff = 50
c ...
    igeom = 3
    nzones = 20
    radmin = 0.
    radmax = 5.37e-2
    dradmn = 5.e-7
c ...
    tempel(1) = 20*300.,
    densnn(1) = 20*1.0836e19
c ...
    atomnm = 13.
    atomwt = 27.0
    ilinep = 1
c ...
    Al XIII H-like
    iselct(1256,1) = 2*1
c
$end

```

RADIATIVE TRANSFER PARAMETERS

isw6=1 => start with LTE populations
 isw6=2 => start with coronal populations
 isw6=3 => set populations to LTE values
 isw6=4 => set populations to coronal values

skip reading of fluorescence yields and Auger rates

PLOTTING SWITCHES

SPECTRAL GRID PARAMETERS (energies in eV)

GRID PARAMETERS (radii in cm)

grid temperatures and ion densities

ATOMIC DATA PARAMETERS

SELECT LEVELS

Figure 9.4. Namelist input for Example 2.

2-Level Atom Source Function
Homogeneous Spherical Plasma

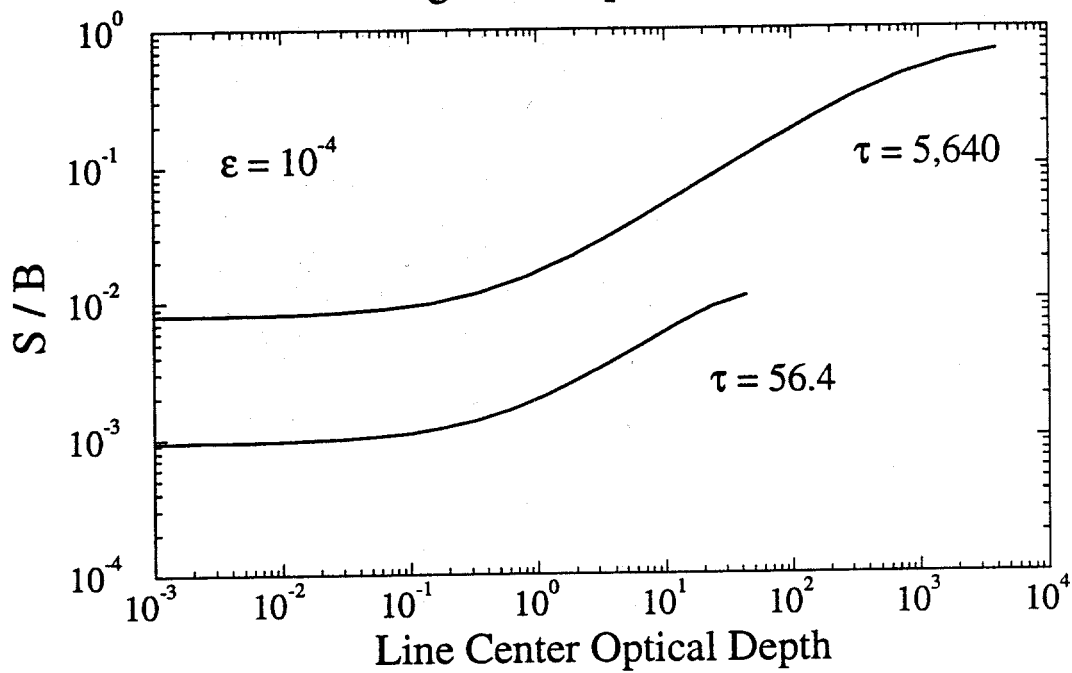


Figure 9.5. Two-level atom source function vs. line center optical depth for Example 2.

```

$input1
c ...                                INITIAL POPULATIONS
c   isw6=1 => start with LTE populations
c   isw6=2 => start with coronal populations
c   isw6=3 => set populations to LTE values
c   isw6=4 => set populations to coronal values
c     isw(6) = 3
c ...
c   iplot(1) = 1                         PLOTTING SWITCHES
c   iplot(8) = 4, 4,
c ...
c   hvmin = 1480.                        SPECTRAL GRID PARAMETERS (energies in eV)
c   hvmax = 1620.
c   nfrqbb = 3
c   nfrqff = 1000
c ...
c   igeom = 1                            GRID PARAMETERS
c   nzones = 1
c   radmin = 0.
c   radmax = 6.75e-4
c   dradmn = 2.e-6
c ...
c   tempel(1) = 1*58.,                  grid temperatures and ion densities
c   densnn(1) = 1*4.4e20
c ...
c   atomnm = 13.                         ATOMIC DATA PARAMETERS
c   atomwt = 27.0
c   ilinep = 3
c ...
c   thermal states                      autoionizing states (n=2)      autoionizing states (n=3)
c   -----
c   Al I                               iselct( 1,1) = 4*0
c   Al II                             iselct( 11,1) = 16*0
c   Al III                           iselct( 34,1) = 3*0
c   Al IV    Ne-like                 iselct(133,1) = 10*0
c   Al V     F-like                 iselct(243,1) = 15*0
c   Al VI    O-like                 iselct(402,1) = 20*1
c   Al VII   N-like                 iselct(614,1) = 44*1
c                                     iselct(682,1) = 8*1           iselct(690,1) = 10*1
c   Al VIII   C-like                iselct(791,1) = 34*1           iselct(836,1) = 16*1           iselct(852,1) = 10*1
c                                     iselct(949,1) = 21*1           iselct(977,1) = 35*1           iselct(1012,1) = 10*1
c   Al IX    B-like                 iselct(1046,1) = 24*1           iselct(1070,1) = 31*1           iselct(1101,1) = 10*1
c   Al X     Be-like                 iselct(1142,1) = 8*1            iselct(1157,1) = 15*1           iselct(1172,1) = 10*1
c   Al XI    Li-like                 iselct(1220,1) = 7*1
c   Al XII   He-like                 iselct(1248,1) = 3*1
c   Al XIV   Fully Ionized        iselct(1258,1) = 1*0
$cend

```

Figure 9.6. Namelist input for Example 3.

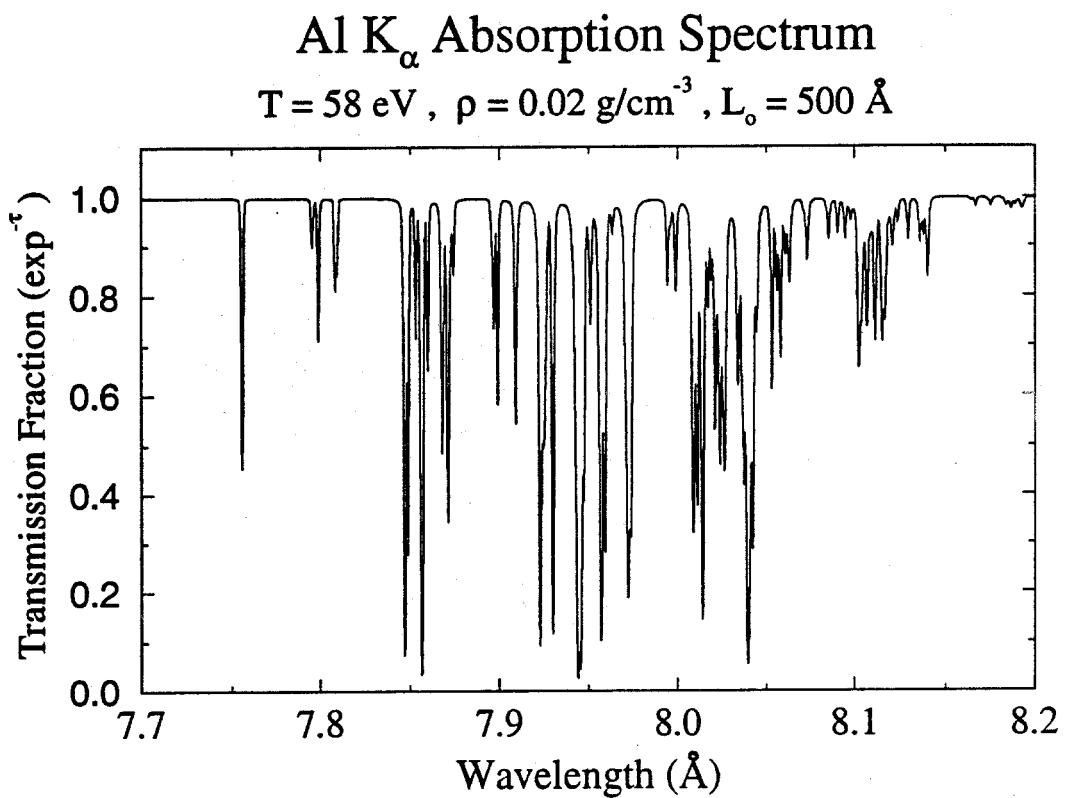


Figure 9.7. Al K _{α} absorption spectrum for Example 3.

Acknowledgments

This work has been supported by Kernforschungszentrum Karlsruhe through Fusion Power Associates.

References

- [1] A. Hauer, R.D. Cowan, B. Yaakobi, O. Barnouin, and R. Epstein, *Phys. Rev. A* **34**, 411 (1986).
- [2] C. Chenais-Popovics, C. Fievet, J.P. Geindre, J.C. Gauthier, E. Luc-Koenig, J.F. Wyart, H. Pepin, and M. Chaker, *Phys. Rev. A* **40**, 3194 (1989).
- [3] J. Bruneau, C. Chenais-Opoovics, D. Desenne, J.-C. Gauthier, J.-P. Geindre, M. Klapisch, J.-P. Le Breton, M. Louis-Jacquet, D. Naccache, and J.-P. Perrine, *Phys. Rev. Lett. Phys. Rev. Lett.* **65**, 1435 (1990).
- [4] S.J. Davidson, J.M. Foster, C.C. Smith, K.A. Warbutron, and S.J. Rose, *Appl. Phys. Lett.* **52**, 847 (1988).
- [5] D.M. O'Neil, C.L.S. Lewis, D. Neely, and S.J. Davidson, *Phys. Rev. A* **44**, 2641 (1991).
- [6] J. Abdallah, Jr., R.E.H. Clark, and J.M. Peek, *Phys. Rev. A* **44**, 4072 (1991).
- [7] T.S. Perry, S.J. Davidson, F.J.D. Serduke, D.R. Bach, C.C. Smith, J.M. Foster, R.J. Doyas, R.A. Ward, C.A. Iglesias, F.J. Rogers, J. Abdallah, Jr., R.E. Steward, J.D. Kilkenny, and R.W. Lee, *Phys. Rev. Lett.* **67**, 3784 (1991).
- [8] C.J. Keane, B.A. Hammel, D.R. Kania, J.D. Kilkenny, R.W. Lee, A.L. Osterheld, L.J. Suter, R.C. Mancini, C.F. Hooper, and N.D. Delameter, *Phys. Fluids* **B 5**, 3328 (1993).
- [9] J. Bailey, A.L. Carlson, G. Chandler, M.S. Derzon, R.J. Dukart, B.A. Hammel, D.J. Johnson, R.R. Lockner, J. Maenchen, E.J. McGuire, T.A. Mehlhorn, W.E. Nelson, L.E. Ruggles, W.A. Stygar, and D.F. Wenger, *Lasers Part. Beams* **8**, 555 (1990).
- [10] J. Bailey, 6th International Workshop on Atomic Physics for Ion-Driven Fusion, Santa Fe, NM, November 1993.
- [11] J.J. MacFarlane, P. Wang, J. Bailey, T.A. Mehlhorn, R.J. Dukart, and R.C. Mancini, *Phys. Rev. E* **47**, 2748 (1993).
- [12] J.J. MacFarlane, P. Wang, T.A. Mehlhorn, J. Bailey, and R.J. Dukart, *Rev. Sci. Instrum.* **63**, 5062 (1992).

- [13] J.J. MacFarlane, P. Wang, and G.A. Moses, Fusion Power Associates Report No. FPA-90-1, January 1990.
- [14] J.J. MacFarlane, P. Wang, and D.L. Henderson, Fusion Power Associates Report No. FPA-91-1, January 1991.
- [15] J.J. MacFarlane, P. Wang, and D.L. Henderson, Fusion Power Associates Report No. FPA-92-1, January 1992.
- [16] J.J. MacFarlane, P. Wang, D.L. Henderson, and O. Yasar, Fusion Power Associates Report No. FPA-93-1, January 1993.
- [17] P. Wang, ATBASE Users' Guide, Fusion Power Associates Report No. FPA-93-7, December 1993.
- [18] E. Anderson et al., LAPACK Users' Guide (SIAM, Philadelphia, 1992).
- [19] K. Werner and D. Husfield, *Astron. Astrophys.* **148**, 417 (1985).
- [20] J.J. MacFarlane, *Astron. Astrophys.* **264**, 153 (1992).
- [21] K.C. Ng, *J. Chem. Phys.* **61**, 2680 (1974).
- [22] L. Auer, in Numerical Radiative Transfer, edited by W. Kalkoten, Cambridge University Press, Cambridge, U.K. (1987), p. 101.
- [23] D. Mihalas, Stellar Atmospheres, Second Edition, Freeman and Company, New York (1978).
- [24] J.P. Apruzese, J. Davis, D. Duston, and K.G. Whitney, *J.Q.S.R.T.* **23**, 479 (1980).
- [25] J.P. Apruzese, *J.Q.S.R.T.* **25**, 419 (1981).
- [26] J.P. Apruzese, *J.Q.S.R.T.* **34**, 447 (1985).
- [27] W.J. Karzus and R. Latter, *Ap. J. Suppl. Ser.* **6**, 167 (1961).
- [28] G.B. Rybicki and D.G. Hummer, *Astron. Astrophys.* **245**, 171 (1991).
- [29] M. Abramowitz and I.A. Stegun, Handbook of Mathematical Functions, Dover Press, New York (1972).
- [30] D. Mihalas, P.B. Kunacz, and D.G. Hummer, *Astrophys. J.* **202**, 465 (1975).
- [31] P. Wang, Ph.D. Dissertation, Dept. of Nuclear Engineering and Engineering Physics, University of Wisconsin, Madison, WI (1991).
- [32] A. Burgess and M.C. Chidichchimo, *Mon. Not. R. Astron. Soc.* **203**, 1269 (1983).

- [33] M.J. Seaton, in Atomic and Molecular Processes, edited by D.R. Bates, Academic, New York (1962) p. 374.
- [34] I.I. Sobelman, L.A. Vainshtein, and E.A. Yukov, Excitation of Atoms and Broadening of Spectral Lines, Springer-Verlag, New York (1981).
- [35] D.E. Post, R.V. Jensen, C.B. Tarter, W.H. Grasberger, and W.A. Lokke, *At. Data Nucl. Data Tables* **20**, 397 (1977).
- [36] E. Merzbacher and H.W. Lewis, in Corpuscles and Radiation in Matter II, edited by S. Flugge, Handbuch der Physik, Vol. 34, Springer-Verlag, Berlin (1958).
- [37] J.J. MacFarlane and P. Wang, Theoretical Spectral Diagnostics Analyses in Support of PBFA-II Beam-Plasma Interaction Experiments, University of Wisconsin Fusion Technology Institute Report No. UWFDM-913, March 1993.
- [38] P.B. Kunacz and D.G. Hummer, *Mon. Not. Royal Astr. Soc.* **166**, 19 (1974).
- [39] G. Athay, Radiation Transport in Spectral Lines, Reidel Publishing, Dordrecht (1972).
- [40] D.G. Hummer, *Mon. Not. Royal Astr. Soc.* **138**, 73 (1968).
- [41] D.G. Hummer and S.A. Voels, *Astron. Astrophys.* **192**, 279 (1988).